Accepted Manuscript

Journal of the Geological Society

Foreland deformation of Brasiliano orogens at the eastern and western margins of the São Francisco Craton: K-Ar illite dating of the Araçuaí and Brasília fold-and-thrust belts

G.A.C. Campanha, M. Hueck, K. Wemmer, M.C.B. Esteves, H.C. Joncew, F.M. Faleiros & R.S.S. Veloso

DOI: https://doi.org/10.1144/jgs2025-138

To access the most recent version of this article, please click the DOI URL in the line above. When citing this article please include the above DOI.

This article is part of the New perspectives on South American Geology: a tribute to Emeritus Professor Reinhardt A. Fuck collection available at: https://www.lyellcollection.org/topic/collections/new-perspectives-on-south-american-geology

Received 29 June 2025
Accepted 17 July 2025

Supplementary material at https://doi.org/10.6084/m9.figshare.c.7951610

Foreland deformation of Brasiliano orogens at the eastern and western margins of the São Francisco Craton: K-Ar illite dating of the Araçuaí and Brasília fold-and-thrust belts

Foreland deformation of Brasiliano orogens

G.A.C. Campanha(1)(*), M. Hueck(2), K. Wemmer(3), M.C.B. Esteves(1), H.C. Joncew(1), F.M. Faleiros(1), R.S.S. Veloso(1)

(1) Institute of Geosciences, University of São Paulo; Rua do Lago 562, Butantã, São Paulo-SP, Brazil, CEP 05508-080

(2) Institute for Geology, Mineralogy and Geophysics, Ruhr-University Bochum; Universitätsstraße 150, 44801 Bochum, Germany

(3) Geoscience Center, Georg-August University Göttingen, Goldschmidtstr. 3, 37077 Göttingen, Germany

(*) Correspondence: ginaldo@usp.br

Abstract

The São Francisco Craton played a central role in the evolution of the Brasiliano Orogeny, with significant deformation along its eastern and western margins forming the Araçuaí and Brasília fold-and-thrust belts. This study investigates the timing and conditions of deformation in the upper crust of these belts using K-Ar illite dating and X-ray diffraction analysis from sedimentary covers in four regions. Samples were collected from Mesoproterozoic (Espinhaço Supergroup and Paranoá Group) and Ediacaran to Cambrian (Bambuí Group) units, in the western São Francisco Craton border (Unaí area, Brasília Belt) and eastern São Francisco Craton border (Araçuaí Belt). Results show that inherited detrital components significantly influence the isotopic system in the Unaí area, with deformation under lower temperatures (anchizonal conditions, ca. 250-270°C), and yielded older, likely mixed, Ediacaran ages that establish a maximum limit age for deformation of ca. 615–570 Ma. In contrast, K-Ar ages from the eastern São Francisco Craton margin range from ca. 510 to 455 Ma establishing a minimum limit age for cooling in epizonal conditions (ca. 350-250°C). The development of oppositely-verging, thin-skinned thrust systems is explained by a Coulomb wedge model, driven by tectonic compression from the Brasiliano Orogeny and gravitational forces from adjacent orogenic mountain building.

In spite of the ubiquity of near-surface processes in the geological record, the application of geochronology to deformation in the upper crust is still an underdeveloped topic. This environment, characterized by anchimetamorphic to lower greenschist facies temperature conditions and a dominance of brittle deformation, is traditionally regarded as the domain of thermochronology (Ault et al., 2019; Gautheron et al., 2022). However, while thermochronology is in many cases able to reconstruct detailed long-term thermal histories of the analysed samples, establishing absolute geochronological constraints for discrete deformation is a challenging task, as the link between structural features and their impact on the involved isotopic systems is often unclear. Among the many complications are factors such as the heterogeneous localization of strain at different scales, the outsized influence of fluid percolation, and the superposition of deformation from polyphasic or progressive deformation (e.g., Oriolo et al., 2018, 2022; Fossen et al., 2019; Bosse & Villa 2019; Roberts et al., 2021). In order to address these issues, it is necessary to acquire age data that can be interpreted in terms of syn-deformation crystallization or isotopic re-equilibration, i.e., that can be described as a petrochronometer (e.g., Engi et al., 2017). The geochronology of illite, i.e., clay-sized white mica that is stable relative to muscovite under temperatures below ca. 300°C, is currently the most established method for obtaining crystallization ages associated to deformation in the upper crust (Hueck et al., 2022). In spite of a relative challenge in interpreting acquired dates that often rely on case-by-case analysis, the method has been successfully applied over the past decades to constrain processes such as brittle faulting, anchimetamorphic folding, and the cooling through the transition of ductile to brittle deformation in reactivated structures in many different settings (van der Pluijm et al., 2001; Fitz-Díaz and van der Pluijm, 2013; Mora et al., 2013; Ksienzyk et al., 2016; Viola et al., 2016; Garduño-Martínez et al., 2015; Hueck et al., 2017, 2020; Süssenberger et al., 2018a; Silva Lara et al., 2021; Monié et al., 2024).

The São Francisco craton is a stable piece of continental crust that has remained mostly undeformed since the Paleoproterozoic. During the Neoproterozoic, the craton was surrounded by various orogenic belts formed during the Brasiliano Orogeny, which was associated with the closure of oceanic basins and the collision of continental fragments during the assembly of Western Gondwana (Almeida, 1977; Heilbron et al., 2017). This process resulted in significant crustal shortening, leading to the development of fold-and-thrust belts along the craton margins. In our region of interest in the South-Central São Francisco Craton, these fold-and-thrust belts include the Brasília Belt to the west and the Araçuaí Belt to the east (Fig. 1 and 2).

In order to estimate the deformation ages and metamorphic conditions related to the foreland covers and marginal fold-and-thrust belts of the São Francisco craton, samples were analysed by K-Ar dating aided by microstructural observations and detailed XRD characterization.

Four areas were studied, encompassing Mesoproterozoic (Espinhaço Supergroup and Paranoá Group), and Ediacaran to Cambrian (Bambuí Group) sedimentary covers along the margins of the São Francisco Craton, with the Brasília (west) and Araçuai (east) belts. These areas include, Unaí, located in the Brasília belt, and the Curimataí-Buenópolis, Rodeador and Serra do Cipó areas, along the Araçuaí belt (Figs. 1 and 2).

Fig. 1. a) Map of the Western Gondwana at ca. 540 Ma with indications of cratons and orogenic belts (in pale-yellow: Brasiliano-Pan African Belts- A: Araçuaí; Ar: Araguaia; B: Brasília; Bb: Borborema; DF: Dom Feliciano; P: Paraguai; R: Ribeira. In grey: Cratons- A: Amazon; C: Congo; K: Kalahari; P: Paranapanema; SF: São Francisco; RP: Rio de la Plata; WA: West Africa); (b) Regional geological map of the São Francisco Craton and surrounding belts (modified from Alkmim et al., 2006), with the Fig. 2 indicated by a yellow box and the study areas by red boxes.

The selected study areas represent autochthonous to parautochthonous sedimentary covers of the São Francisco Craton involved in two thin-skinned fold-and-thrust belts with opposing vergences, affected by mostly coeval Neoproterozoic/Cambrian orogens on both sides of the craton. By applying K-Ar illite dating aided by microstructural observations and detailed XRD characterization of samples from the sedimentary covers along the craton eastern and western margins, this study aims to provide new temporal constraints on deformation events and unravel the thermal history along the São Francisco Craton margins. The results not only enhance our understanding of the São Francisco Craton's tectonic role as a rigid boundary to the orogenic advance but also contribute to ectonics and sedimentation during orogenesis.

Fig. 2 – Simplified geologic map of the South-Central portion of the São Francisco craton (modified from Serviço Geológico do Brasil, 2025).

Geological setting

The São Francisco Craton is the peninsular portion of the São Francisco-Congo paleocontinent delimited by Brasiliano/Panafrican orogenic belts evolved during the formation of

the Western Gondwana supercontinent (Fig. 1) (Almeida, 1966, 1977; Alkmim et al., 1993; Alkmim, 2004). Collisions to the east rotated the peninsula towards the continent, resulting in the construction of the Araçuaí-West Congo orogen (Alkmim, 2006; Pedrosa-Soares et al., 2001), while to the west the Brasília Belt was formed during the Edicaran convergence of the Amazonian, São Francisco-Congo, Paranapanema and Rio de La Plata cratons (Fuck et al., 2008; Pimentel, 2016).

The central and southern portion of the São Francisco Craton is covered by the homonymous São Francisco Basin (Chang et al., 1988; Campos and Dardenne, 1997), which accumulated sediments in the Paleo-, Meso- and Neoproterozoic, Carboniferous and Cretaceous periods (Fig. 2). The tectonic evolution of the basin is polyphasic, with orogenic pulses in the Paleo- and Neoproterozoic, and taphrogenic pulses in the Statherian, Tonian, and Cretaceous. (Alkmim and Martins-Neto, 2001; Martins-Neto et al., 2001)

The sedimentary cover includes i) the Statherian to Stenian Espinhaço Supergroup, in the central and eastern portion of the São Francisco Craton, as well as the Paranoá and Araí groups at the western border, representing rift to rift-sag basins (Martins-Neto., 1998; Chemale et al., 2011, 2012); (ii) the Tonian to Criogenian Macaúbas Group and Jequitaí Formation, associated with a Neoproterozoic rift-passive margin contemporaneous with the Rodinia breakup and a continental glaciation (Pedrosa-Soares et al., 1992, 1998, 2001, 2007; Pedrosa-Soares and Alkmim, 2011); (iii) the Ediacaran to Cambrian Bambuí Group, related to a foreland system associated with the Brasiliano/PanAfrican West Gondwana assembly (Dardenne, 1978; Chang et al., 1988); and (iv) Permo-Carboniferous, Cretaceous and Cenozoic units, a continental extensional system related to the Pangea breakup and the South Atlantic opening (Campos and Dardenne, 1997) (Fig. 2 and 3).

The classic exposure area of the Espinhaço Supergroup is in the marginal portion of the Araçuaí Belt, known as the Southern Espinhaço Range, where its standard lithostratigraphic subdivision was originally defined (Fig. 4). The unit also crops out in some large brachyanticlines and seismic sections and well data indicate its continuity at depth in the central portion of the São Francisco Craton (Reis et al., 2017; Martins-Ferreira, 2020).

The Tonian to Cryogenian Macaúbas Group and the Jequitaí Formation lie unconformably over the Espinhaço Supergroup. The Jequitaí Formation is defined as a glacial-related succession deposited on the São Francisco Craton, whereas the Macaúbas Group represents a more complex, chronocorrelated succession developed within the Araçuaí Belt. For the purposes of this study and within the areas considered, the Macaúbas Group is treated as undivided.

The Ediacaran to Cambrian Bambuí Group covers the largest area of the São Francisco Basin. It comprises a package of carbonates, pelites, sandstones, and subordinate conglomerates, subdivided into five main formations (Fig. 4). The term Paraobeba Subgroup is used in areas where distinguishing the lower formations is not possible.

Fig. 3 - Chronostratigraphic chart for the Proterozoic to Cambrian major units from the South-Central São Francisco craton and marginal fold-and-thrust belts (modified from Alkmim and Martins-Neto, 2012; Reis et al., 2017; Medeiros et al., 2024; Dias et al., 2025).

Radiometric ages obtained by Pb/Pb method for the Bambuí Group dated the basal carbonate cap of the Sete Lagoas Formation at 740 ± 22 Ma (Babinski et al., 2007). However, a significant number of U-Pb analysis in detrital zircon for all formations of this Group showed a strong contribution of material dated to the end of the Neoproterozoic until the Cambrian, spanning from 635 to 513 Ma (e.g. Rodrigues, 2008; Pimentel et al., 2011; Paula-Santos et al., 2015, 2017; Pimentel, 2016; Uhlein et al., 2017; Kuchenbecker et al., 2020; Moreira et al., 2020; Tavares et al., 2020; Caxito et al., 2021), with the largest peak with ages around 620 Ma, and the youngest reaching 513 Ma. In addition, an Ediacaran fossiliferous assemblage (about 540 Ma) was identified by Warren et al. (2014). These data demonstrate that the deposition of the Bambuí Group occurred near the end of the Neoproterozoic and beginning of the Cambrian, a short time after the peak of metamorphism recorded in the Brasília and Araçuaí belts, reinforcing the idea that such deposits represent a foreland basin in relation to the final evolution of the orogen, as previously suggested by Chang et al. (1988).

Concerning its Proterozoic to Cambrian covers, the São Francisco Basin can be divided into three structural compartments. While the central zone is practically undisturbed, the edges configure a dual system of marginal fold-and-thrust belts with opposite tectonic vergences to the Craton interior and thin-skinned tectonics affecting the sedimentary cover (Alkmim et al., 1996; Alkmim & Martins-Neto, 2001; Reis et al., 2017; Martins-Ferreira, 2019).

Fig. 4 -Stratigraphic column and main radiometric data for the Espinhaço and São Francisco supergroups, with emphasis on the studied areas, being the Macaúbas Group considered as undivided. YZG – youngest zircon grain. Citations: (1)-Tavares et al., 2020; (2)-Kuchenbecker et al., 2020; (3) Rodrigues, 2008; (4) Moreira et al., 2020; (5) Paula-Santos et al., 2017; (6) Chemale et al., 2012; (7) Lopes 2012; (8) Babinski et al., 2007 (Pb-Pb); 9-Warren et al., 2014 (Cloudina sp.); 10-Machado et al., 1989; (11) Queiroga et al., 2012; (12) Souza, 2016; (13) Brito Neves et al., 1979. (Modified from Alkmim et al., 2017; Reis et al., 2017).

Unaí area

The Unaí area lies on the limit between the Brasília Belt and the western margin of the São Francisco Craton (Fig. 5). It is dominated by the sedimentary covers of the Mesoproterozic Paranoá Group and the Ediacaran to Cambrian Bambuí Group. The Bambuí Group in this area is constituted by the Sete Lagoas, Serra de Santa Helena and Serra da Saudade formations, as well the undivided Paraopeba Subgroup, in which metalimestone, metadolomite, metasiltstone and metasandstone are the predominant lithotypes. Most of the central portion of the studied area is composed by the undivided Paraopeba Subgroup, while the Paranoá Group is exposed in anticline cores, comprising mainly sandstones, locally conglomeratic, with intercalations of siltstones. The regional structure is characterized by NNE-trending thrust zones and east-verging normal-horizontal folds. Regional seismic sections reveal that the foreland fold-thrust belt involving the Bambuí Group rocks is detached over a subhorizontal basement surface in a thin-skinned tectonic pattern (Coelho et al. 2008; Martins-Ferreira 2019). Beneath this east-verging thin-skinned fold-thrust zone, in surface exposures, siliciclastic and carbonate rocks of the Bambuí and Paranoá groups commonly display upright chevron and box folds (Fig. 6a), which are progressively superseded by isolated kink bands towards the central portion of the craton, folding the sedimentary bedding and developing a fine continuous cleavage in plane-axial position (Reis et al., 2017; Martins-Ferreira, 2019; Esteves and Faleiros, 2021).

Subhorizontal extensional veins hosted by the low-grade metasedimentary rocks of the Bambuí Group formed under subhorizontal shortening and subvertical extension, supporting vein development under a fold-thrust regime that formed the regional NW-trending thrusts and megafolds (Esteves and Faleiros, 2021).

Fig. 5 – Geologic map and cross-section for the Unaí area (Modified from Baptista et al, 2015, Esteves and Faleiros, 2021).

Fig. 6 – Field pictures of the studied: a) chevron folds on metapelites from the Bambuí Group, Paraopeba Subgroup, Unaí area; b) moderately-dipping sedimentary bedding crossed by an upright slate cleavage on metapelites from the Serra de Santa Helena Formation, Bambuí Group, Buenópolis area; c) stretching lineations on metasandstones form the Córrego Pereira Formation, Espinhaço Supergroup, Rodador area; d) overturned fold on metapelites from the Serra de Santa

Helena Formation, Bambuí Group, near Serra do Cipó area. e) metadiamictites from the Macaúbas Group, Buenópolis area; f) ripple marks on metasandstones from the lower Espinhaço Supergroup, Serra do Cipó area.

Curimataí-Buenópolis area

This area encompasses the eastern limb of the Serra do Cabral anticline to the west, the Buenópolis syncline in the center, and a brachyanticline of the Serra do Espinhaço range (locally referred to as "Serra Mineira") to the east (Fig. 7).

The outcropping units are the Espinhaço Supergroup (Galho do Miguel, Santa Rita, and Córrego dos Borges formations), the Macaúbas Group (including the Jequitaí Formation) (Fig. 6e), and the Bambuí Group (Serra de Santa Helena, Lagoa do Jacaré, Serra da Saudade, and Três Marias formations). The metamorphic grade in all units is very low, with open folds, sometimes with a fine steep slaty cleavage oriented roughly N-S and dipping eastward (Fig. 6b). The original stratigraphic stacking and sedimentary features are preserved in all units.

A low-angle angular unconformity between gently dipping layers of the Macaúbas Group and the Espinhaço Supergroup is reported by several authors (e.g., Moraes, 1937; Köster, 1984; Almeida-Abreu and Renger, 2002) and can be directly observed in the field. The main thrust of the Espinhaço Supergroup over the Neoproterozoic units occurring further south, such as in Rodeador and Serra do Cipó areas, considered as the conventional São Francisco Craton /Araçuaí Belt limit, does not extend into this area.

Fig. 7 – Geologic map and cross-section for the Curimataí - Buenópolis area (Modified from Köster, 1984, Noce, 1997, Fogaça, 1997, Martins et al., 2011, Knauer et al., 2011).

Rodeador area

The region between the districts of Rodeador and Conselheiro Mata is marked by the main thrust fault of N-S direction dipping to the east, which thrusts units of the Espinhaço Supergroup over units of the Macaúbas and Bambuí groups (Fig. 8). The Espinhaço Supergroup is constituted locally by the Córrego Pereira and Rio Pardo Grande formations (Conselheiro Mata Group), which are cut by metabasic dikes from the Pedro Lessa Suite. The Macaúbas Group, on the other hand, is constituted by the Duas Barras Formation, and the Bambuí Group by the Sete Lagoas and Serra de

Santa Helena formations. Near the main thrust, the units of the Bambuí and Macaúbas groups are strongly deformed with a pervasive schistosity with stretching lineations and kinematic indicators, such as asymmetric boudins and porphyroclasts, pointing to a west-verging tectonics (Fig. 6c). To the east and far from the main thrust, the main structure of the Espinhaço domain is dominated by large-scale open folding of the sedimentary bedding, with development of an oblique slate cleavage. Greenschist facies metamorphism is associated with the deformation (Fogaça, 1997; Knauer et al., 2011, 2014; Araujo et al, 2020).

Fig 8 - Geologic map and cross-section for the Rodeador area (Modified from Fogaça, 1997, Araújo et al., 2020).

Serra do Cipó area

The Serra do Cipó area includes the boundary between the São Francisco Craton (west) and the Araçuaí Belt (east), defined by a major thrust putting Mesoproterozoic rocks from the upper Espinhaço Supergroup over Ediacaran-Cambrian rocks of the Bambuí Group (Fig. 9).

The macrostructure comprises thrust slices from the Espinhaço Supergroup units, recognized as tectonic repetitions of the Galho do Miguel and Santa Rita formations, thrust over units of the Bambuí Group, (Sete Lagoas, and Serra de Santa Helena formations). The area can be divided in two tectonic domains, a fold-and-thrust belt to the east, and a foreland domain, to the west, both characterized by west-verging tectonics. The fold-and-thrust belt domain is essentially made up of the Espinhaço Supergroup, strongly deformed. The same unit is also present in the foreland region as a rigid basement to the foreland basin represented by the Bambuí Group.

Local structures at all scales, such as reverse faults, shear zones, asymmetric folds, tectonic foliations, stretching lineations and kinematic indicators, are coherent with the regional westward vergence (Fig. 6d). In the foreland domain, the Espinhaço Supergroup is near undeformed below a detachment surface separating it from the Bambuí Group (Cipó River window) (Fig. 6f), which, in turn, accommodated most of the orogenic deformation.

Fig. 9 - Geologic map and cross-section for the Serra do Cipó area (Joncew, 2024; Joncew et al., 2025).

Methods

The selected samples were characterized by optical microscopy in thin sections and by scanning electron microscope in little rock fragments. Sample preparation and analytical work was performed at the Geoscience Centre of the Georg–August–Universität Göttingen. More details about all analytical procedures are presented in the supplementary material, of which the main elements are presented below. All samples were gently crushed and sieved, and the resulting <63 µm fraction was separated for further grain size fractionation. Clay fractions <2 µm were concentrated using differential settling velocities in Atterberg cylinders following Stoke's Law. A second <2 µm fraction gained the same way was separated for concentrating fractions <0.2 µm following the same principle, and using an ultra-centrifuge to impose higher accelerations and thus significantly reduce settling time for very small particles. Separating a sample's clay fraction into different grain size fractions is desirable as it can be used to investigate whether the analysed material is homogeneous or a mixture of different populations of clay-sized white mica, by investigating variations in the resulting K-Ar ages and XRD data of different fractions from a same fraction (Hueck et al., 2022). Unfortunately, not all samples yielded enough material to perform all analyses in both fractions, particularly in the case of rocks that experienced slightly higher-temperatures (see results and discussion), which typically have a smaller clay content due to the progressive coarsening of crystal sizes with increasing metamorphic degree. XRD analysis was performed in order to identify and quantify the mineralogy of the clay fractions through Rietveld refinement using the BGMN-based Profex software (Doebelin & Kleeberg 2015). In addition, crystallographic features of the dated illite were also determined, namely by estimating illite "crystallinity" (expressed as CIS-corrected Kübler Index (KI), Warr & Ferreiro-Mählmann 2015; Warr 2018) and the relative proportion of different white mica polytypes (expressed in the % of $2M_1$ Illite), both of which are temperature-dependent. For the dating, K and Ar were measured independently from multiple aliquots of the same grain-size fractions. More details about all analytical procedures are presented in the supplementary material.

Results

Sample description

A total of eleven pelitic samples with newly formed cleavage associated to the regional deformation were collected from different stratigraphic units of the foreland covers of the São

Francisco Craton along its SW and SE borders, near the limits with the Brasília and Araçuaí belts, respectively (Table 1, Figs 5 to 9). The samples were selected as the less weathered ones within our areas mapped in detail.

From the western side, near the limit with the Brasília belt, three samples of the Unaí area were selected, UN4 from the Paranoá Group (Mesoproterozoic) and UN14 and UN21 from the Paraopeba Subgroup, Bambuí Group (Ediacaran-Cambrian). All samples comprise metasiltstones with preserved sedimentary structures such as parallel and cross-stratification and a NW–SE continuous cleavage composed of preferentially oriented sericite. The cleavage can appear wavy in the microscale, deflecting along coarser-grained and probably detrital mica crystals (Fig. 10a).

Three samples are from Buenópolis-Curimataí area, at the eastern side near the conventional border between the São Francisco Craton and the Araçuaí Belt. All samples are metasiltstone and preserve sedimentary structures and textures such as a fine sedimentary lamination, as well as a slaty cleavage oblique to the bedding, consisting predominantly of aligned illite and chlorite grains (Fig. 10b). Samples N10 and N43A are from the Serra de Santa Helena Formation, Bambuí Group (Ediacaran-Cambrian). Sample N49 is from the Santa Rita Formation (Conselheiro Mata Group, Espinhaço Supergroup) (Mesoproterozoic), at an area in which it is covered in angular unconformity by the Macaúbas Group (Tonian).

Sample N24 from the Rodeador-Conselheiro Mata area is a metasiltstone, belonging to the Rio Pardo Grande Formation, top unit of the Conselheiro Mata Group, Espinhaço Supergroup (Mesoproterozoic), with well-preserved sedimentary structures such as ripple marks and fine sedimentary lamination, and with a slaty cleavage oblique to the bedding.

Four samples are from the Serra do Cipó area, where a major thrust put the Espinhaço Supergroup over the Bambuí Group. Metasedimentary rocks in this area are stronger deformed when compared with the former areas, as recognized in much more pervasive cleavages in microscale, with a predominance of coarser-grained white mica relative to the other samples. This is also compatible with the small quantity of clay-sized mica that could be extracted from these samples. Nonetheless, the samples are still on the greenschist facies conditions and have preserved sedimentary structures (Fig. 10 c and d). Sample HJ 41 was taken from the Santa Rita Formation (Espinhaço Supergroup) close to the main regional thrust, and corresponds to a fine-grained, laminated quartz phyllite, with well-developed mylonitic schistosity and stretching lineation. Sample HJ 98B is a poorly selected, medium-grained foliated quartzite from the Santa Rita Formation, also close to the main Espinhaço thrust, containing millimetric phyllitic microlithons. Samples HJ 165 and HJ 169 belong to the Serra de Santa Helena Formation (Bambuí Group) and correspond to foliated gray rhythmitic metapelitic rocks with well-marked slaty cleavage parallel to the bedding and gently undulated due to crenulation.

Fig. 10 – Scanning electron microscopy images illustrating microstructural characteristics of selected sample. Images on the left hand, correspond to back-scattered electron images, whereas images on the right hand also incorporate energy-dispersive X-ray spectroscopy information; a) UN21B sample, from Unaí area; b) N43A sample, Curimataí – Buenópolis area; c) HJ165 sample, Serra do Cipó area; d) HJ169 sample, Serra do Cipó area.

XRD mineralogy

Qualitative and quantitative mineralogical characterizations were performed in the analysed samples, as not all of them produced enough quantities of <0.2 μm material for the confection of untextured powder preparations for XRD analysis, which is necessary for a quantitative mineralogical characterization using Rietveld refinement. However, the qualitative analyses performed in textured preparations are in accordance with the quantitative analyses performed for the same samples. Furthermore, for the samples for which it was possible to perform a quantitative mineralogical evaluation in both grain-size fractions (samples N10 and N43A, both from the eastern margin of the São Francisco Craton), the mineralogy of both fractions is compatible with one another, with most differences limited to relative changes in the proportion of the minerals, often with an increase in the proportion of minerals such as goethite, smectite, and chlorite in the finest fraction (supplementary material). Because of that, Fig. 11 provides an overview of the mineralogy of all samples based on the results of the <2 μm fraction.

The fine fractions concentrated for analyses are mostly composed of clay minerals, which in all but one sample (HJ165) comprise more than 80% of the material, and can reach up to >95% in sample UN4. The dominant clay mineral in most samples is illite (sensu latu, meaning that this can include also clay-sized muscovite and phengite, as well as illite-like mixtures with small amounts of smectite, Hueck et al., 2022). Except for sample N49A, which contains ca. 45% of kaolinite, illite accounts for between 55 and 92% of the mineral concentration in all other samples. Kaolinite and chlorite are relatively common constituents (Figs. 10, 11), though they do not occur in all samples, and smectite is only present in one sample (N10), in which it constitutes ca. 20% of the sample. The presence of smectite may affect the K-Ar dates in this sample, as smectite is commonly associated with late alteration of illite at very low temperatures (Meunier & Velde, 2004). On the other hand,

there are virtually no K-bearing mineral phases in addition to illite that could impact the K-Ar dates (e.g., Viola et al. 2013; Torgersen et al. 2015), except for a trace amount of clay-sized K-feldspar (<2%) in sample UN-14 (see discussion about possible implications). Clay-sized quartz and plagioclase are common contaminants in all samples (Fig. 10), as well as trace quantities of Ti-oxides (rutile and anatase), titanite, hematite, and calcite in individual samples (Fig. 10).

Fig. 11. Summary of the mineralogical composition of all analysed samples determined by Rietveld refinement. Samples from the SE border of the São Francisco Craton (São Francisco Craton) are organized approximately from South to North.

Illite characterization

Two commonly used temperature-dependent crystallographic parameters of illite were quantified in the analysed samples, in order to estimate the temperature conditions in which the dated white mica was crystallized, namely illite crystallinity and polytype composition. Illite crystallinity is an empiric value corresponding to the width at half maximum height of the 001 reflection peak of white mica in the XRD spectra of textured samples, also known as Kübler Index, (KI, Kübler, 1967). This peak becomes progressively sharper with increasing temperatures, as crystallographic ordering increases and lattice strain decreases, which also leads to coarser crystallites. Systematic investigations of KI in pelitic sediments (Kübler, 1967; Merriman & Frey, 1999) were used to define the transitions between very low-temperature metamorphic facies, which, in the most recent inter-laboratorial standardization (CIS, Warr, 2018), corresponds to KI values of 0.52 for the transition from diagenesis into anchizone (ca. 200°C), and a KI of 0.32 for the transition from anchizone to epizone. According to Warr (1996), the diagenetic zone can be approximately correlated to the zeolite facies, the anchizone to the prehnite-pumpellyite facies and the pumpelyite-actinolite facies, and the epizone to the beginning of grenschist facies.

The second parameter quantified in the analysed samples is the composition of the different illite polytypes. Different polytypes result from contrasting degrees of ordering of phyllosilicate sheets relative to another within illite crystals (Moore & Reynolds, 1997). This parameter is also temperature-dependent, as more ordered polytypes crystallize with higher temperatures. Whereas different proposals for more or less transitional series between different polytypes have been proposed (see Meunier & Velde, 2004), the most useful geothermometric information derived from the polytypes is the relative proportion of the high-temperature $2M_1$ polytype (Hueck et al., 2022),

which starts restructuring at temperatures above ca. 200°C (Hunziker et al., 1986; Moore & Reynolds, 1997; Merriman & Frey, 1999).

As in the case of the quantitative mineralogy, polytype quantification requires untextured powder preparations for XRD analysis, which was only possible for two samples in the typically smaller <0.2 μm fraction. That said, both KI and polytype composition results of samples for which both grain sizes are available yield consistent results, with the finest fractions producing values that are indicative of lower temperature conditions (Fig. 12, see discussion for implications). In addition, there is a remarkable correlation between KI and %2M_1 values for samples in which both parameters are available (Fig. 12). This suggests that the methods are compatible for this set of samples, and that the differences observed between the samples reflect changes in the temperature conditions during *in-situ* illite crystallization. In this sense, it is advisable to analyse the <2 um fractions for inter-sample comparisons, as this fraction was completely characterized for all samples. This comparison reveals evident differences in the illite characteristics between the samples from SE and SW borders of the São Francisco Craton. The former, represented by three samples from the Unaí area, are characterized by KI values between 0.48 and 0.36, and relatively low contents of the 2M_1 polytype (13 to 22%). Both parameters indicate anchizonal temperature conditions. On the other hand, all three sample areas from the SE border of the São Francisco Craton are characterized by lower KI values and more elevated 2M_1% contents in general, suggesting higher temperature conditions compatible with the Epizone, i.e., in the lower greenschist facies. Whereas there is some inter-sample variability in the polytype characterization of the samples, which can range from ca. 45 to 80%, the KI values for all samples are remarkably consistent between 0.23 and 0.29, despite differences in the stratigraphic unit and structural position (e.g., distance to the main Espinhaço-Bambuí thrust) of the sampling sites. This is relevant because the KI parameter is better established and, overall, more reliable for illite characterization than polytype quantification (Hueck et al., 2022), as it follows an inter-laboratorial standardization (Warr, 2018), and is less sensitive to variations in sample mineralogy (Boles et al., 2018).

Fig. 12. XRD-based illite characterization summarizing CIS-corrected (Warr & Ferreiro-Mählmann, 2015; Warr, 2018) Kübler Indexes (KI) and relative proportions of the 2M_1 illite polytype of all analysed samples. In the first diagrams, samples from the SE border of the São Francisco Craton (São Francisco Craton) are organized approximately from South to North.

K-Ar geochronology

As with the illite characterization, K-Ar results from samples for which both the <2 and <0.2 μm fractions were analysed are predominantly grain-size dependent (Fig. 13). In other words, in most cases, the K-Ar dates of different grain-size fractions from a same sample are separated by a time interval larger than the sum of their uncertainties. This feature is a very common characteristic of illite geochronology in general (Hower et al., 1963; Clauer & Chaudhuri, 1999; Grathoff & Moore, 1996; van der Pluijm et al., 2001), and reflects the fact that illite is a relatively heterogeneous isotopic system (see discussion for implications to the interpretation of the illite dates). Typically, this grain-size dependency results in the finest fraction yielding the youngest ages, which is in fact the case in almost all samples in the present dataset, except for two. Sample N43A, collected in the Curimataí-Buenópolis area, produced essentially the same age (ca. 455 Ma) for both analysed samples, indicating a more homogeneous illite isotopic system in this sample. On the other hand, sample UN14, from the Unaí area, yields a more unexpected inverse pattern, that is, in which the <0.2 μm fraction produced a K-Ar date (ca. 613 Ma) that is older than that of the <2 μm (ca. 600 Ma), which only barely overlap within uncertainty (Fig. 13, see discussion for interpretation).

Once more, there is a clear difference between the results from the SW and SE border of the São Francisco Craton. Samples from all three areas of the SE border yield Cambrian to Ordovician ages between ca. 510 and 436 Ma. Considering only the <2 μm fractions, which are more appropriate for inter-sample comparison as they were analysed in all samples, this interval is only slightly larger, from ca. 510 to 455 Ma. There is a wide overlap between the date interval obtained in the southernmost area (Serra do Cipó) and the more northern areas (Rodeador and Curimataí-Buenópolis), with both yielding essentially indistinguishable results. There is also no apparent correlation between ages and stratigraphic unit or structural position of the sampling site. In contrast, results from the Unaí area in the SW border of the São Francisco Craton are much older (Ediacaran), but also extend for a large time interval between ca. 644 and 600 Ma for the <2 μm fractions and ca. 613 to 569 Ma for the <0.2 μm fractions.

Fig. 13. Summary of K-Ar ages of all analysed samples organized according to location and compared against CIS-corrected Kübler Index (KI). In the first diagram, samples from the SE border of the São Francisco Craton (São Francisco Craton) are organized approximately from South to North.

Discussion

Interpretation of illite geothermometry and geochronology

The interpretation of illite K-Ar geochronology is challenging due to the typical isotopic heterogeneity of the analysed material, best exemplified by its characteristic grain-size dependency of K-Ar dates, which are usually younger for the finest analysed fractions and older for the coarsest ones (Hower et al., 1963; Clauer & Chaudhuri, 1999; Grathoff & Moore, 1996; van der Pluijm et al., 2001). This heterogeneity derives predominantly from two sources (see review in Hueck et al., 2022): 1- the presence of a physical mixture of different illite generations within a same sample; and 2- grain-size dependent partial loss of radiogenic argon.

A heterogeneous mixture of different illite populations can be caused by a poly-phase low-temperature metamorphic history (Nierhoff et al., 2011; Süssenberger et al., 2018a) or, more likely in the case of low-grade metasedimentary rocks, by the presence of a certain amount of detrital clay-sized white mica inherited form the rock's sedimentary sources (Reuter & Dallmeyer, 1989; Fitz-Díaz & van der Pluijm, 2013; Schomberg et al., 2019). On the other hand, grain-size dependent argon loss occurs when the rock is exposed to temperatures close to the K-Ar closure temperature in illite, leading to a partial loss of radiogenic Ar that is controlled by volume diffusion and, consequently, is dependent on the size of the considered grain (Parry et al., 2001; Zwingmann et al., 2010; Verdel et al., 2012). The closure temperature of clay-sized illite, determined by the extrapolation of Ar diffusion parameters for coarse-grained muscovite defined experimentally (Harrison et al., 2009; Duvall et al., 2011; Rahl et al., 2011), and supported by various empirical studies (Hunziker et al., 1986; Verdel et al., 2012; Wemmer & Ahrendt, 1997; Süssenberger et al., 2018b), is estimated to cover a large interval between 250-350 °C, depending on the grain size.

The incorporation of detrital illite, as observed in SEM imaging of these sample (Fig.10), is likely to be responsible for the grain-size dependency observed in the samples from the Unaí Area (SW São Francisco Craton border), as well as for their comparably old ages. Both illite geothermometry and independent temperature estimates (Esteves & Faleiros, 2021) indicate peak Anchizonal temperature conditions of ca. 250-270°C during deformation, which is within the lower range of the partial diffusion zone of Ar in illite (see above). Hence, it is very likely that the detrital mica population in the sediments retain a significant portion of the radiogenic Ar accumulated since the original exhumation of their sedimentary source areas. Because the analysed samples come from the Paranoá (Mesoproterozoic) and Bambuí (Ediacaran-Cambrian) groups, this means that any amount of Ar budget inherited from detrital illite grains in these samples should have an outsized impact in the resulting dates. This is despite the indication from the mineralogical quantification that no more than ca. 20% of the analysed illite in these samples is of the high-temperature $2M_1$

polytype. Because this is the polytype most resistant to sedimentary transport (Grathoff et al. 2001), it gives an estimate of the maximum amount of detrital illite in the sample, though the temperatures experienced by these rocks make it very likely that some of this polytype also crystallized *in situ* during deformation. In any case, because of the impact of Ar inheritance in these samples, the best possible interpretation that can be obtained from the samples in the Unaí Area is that the dates from the finest fractions (<0.2 μm, ca. 615 to 570 Ma), which should have the smallest possible detrital component (Hueck et al., 2022), provide a maximum age for the deformation and authigenic illite growth in the analysed samples. Another important observation from the Unaí Area is the inverse age pattern of sample UN14, that is, with the finest fraction yielding slightly older ages than the coarser fraction (ca. 613 and 600 Ma, respectively). This observation may reflect the presence of very small quantities of detrital K-feldspar in the <2 μm fraction (ca. 2%), which was not observed in the qualitative XRD spectra for the <0.2 μm fraction. Because this mineral has a lower closure temperature than illite (ca. 150 - 300°C, McDougall & Harrison, 1999) it is possible that a more pronounced loss of Ar in inherited K-feldspar resulted in a younger K-Ar date.

In contrast to the results from the SW border of the São Francisco Craton, illite thermometry from samples of the SE border of the craton indicate significantly higher temperature conditions within the Epizone. This is in accordance with the much better developed cleavages marked by coarser-grained mica present in these samples in the microscale (Fig. 10), as well as with independent temperature estimates extending well into the greenschist facies for the Serra do Cipó Area (Joncew, in review). These conditions are already above the closure temperature of illite (see above), and therefore the resulting ages must be interpreted as cooling ages. In this context, the grain-size dependency of K-Ar dates observed in most samples in which two illite fractions were dated can be a result of grain-size dependent argon loss, or alternatively due to a mixture of illite populations resulting from a protracted history of authigenic crystallization, which is common during deformation in the transition between the ductile and brittle regimes (Kirschner et al. 1996; Löbens et al. 2011; Nierhoff et al. 2011; Hueck et al., 2017, 2020; Süssenberger et al. 2018a). In these cases, the best possible strategy is to assume that the ages from the coarsest fractions (<2 μm, ca. 510 to 455 Ma) establish a minimum (younger) age limit for the cooling through temperature conditions of ca. 350-250°C. Because the peak temperatures estimated in this area are not much higher than this temperature range, it is reasonable to assume that this limit age should not be too distant from the age of deformation itself. This interpretation is in accordance with Hueck et al., (2020), which obtained illite K-Ar between ca. 550 and 450 Ma in the Dom Feliciano Belt in South Brazil that are also strictly cooling ages, but that overlap with the onset of brittle deformation as constrained by the dating of fault gouges in the same structures.

Comparison with former geothermometry and geochronology data

Our illite geothermometry results for the Unaí area are compatible with estimates from Esteves and Faleiros (2021). Thermodynamic models, fluid inclusion analysis and grain-scale deformation accommodated by dissolution-precipitation creep and intracrystalline deformation all indicate metamorphic and deformational conditions of 250–270ºC for the sedimentary rocks of the Unaí area.

Conversely, Joncew (2024) and Joncew et al. (in review) estimated the temperature and pressure during deformation in the Serra do Cipó area based on mineral assemblages, fluid inclusions, deformation mechanisms associated with microstructures, quartz c-axis patterns and illite crystallinity as 300-410 ºC and 1.7-6.0 kbar in the foreland (craton) domain, and 385-450 ºC and 2.8-8.0 kbar in the fold-and-thrust (Araçuaí belt) domain. This is also in accordance with the higher temperature estimates from illite geothermometry in this region.

Our new Cambrian to Ordovician illite K-Ar cooling ages around 510–455 Ma at the São Francisco Craton eastern border are consistent with the depositional ages of the Bambui Group, which range from about 615-513 Ma (e.g., Warren et al. 2014; Paula-Santos et al. 205, 2017; Pimentel 2016; Pimentel et al. 2011; Kuchenbecker et al., 2020; Moreira et al., 2020; Caxito et al., 2021; Tavares et al., 2020) but also suggesting some contemporaneity between the orogenic deformation and the last depositional successions, especially considering that the K-Ar data are interpreted as providing a minimum (younger) age limit in the region.

Two interesting points can be highlighted. Sample HJ98B also has a (coarse-grained) muscovite Rb-Sr i*n situ* age of 548 Ma (Joncew, 2024), which, together with the illite -Ar ages between 476 Ma (fraction <2 μm) and 433 Ma (fraction <0.2 μm) suggest a protracted cooling history. Additionally, in the northern portion of the SE border of the São Francisco Craton, sample N49 belongs to the Santa Rita Formation, in a place where an angular unconformity between the Upper Espinhaço Supergroup with the Macaúbas Group is reported (e.g., Moraes, 1937; Köster, 1984; Almeida-Abreu and Renger, 2002), but our K-Ar results point to a same deformation age over all the area, including the Bambuí and Macaúbas groups and the upper Espinhaço Supergroup. Thus, this angular unconformity is probably related to non-metamorphic upper crustal level deformation of the Espinhaço Supergroup, prior to the Macaúbas deposition, or it was entirely reset for the sensitivity range of K-Ar in illite (below ca. 250-350 °C) in the late Neoproterozoic/Cambrian transition.

For the Espinhaço Supergroup in the northern portion of the São Francisco Craton (Chapada Diamantina Group), Süssenberger et al. (2014) obtained K-Ar illite dates between 470 and 460 Ma

for the inversion and reactivation of the Paramirim Aulacogen, interpreted as related to the Araçuai belt orogenesis, which is consistent with the results presented in this contribution.

Late deformational and metamorphic evolution

The Neoproterozoic to Cambrian foreland fold-and-thrust belts that developed along the southern margins of the São Francisco craton, specifically, the Araçuaí, Brasília, and Ribeira belts, evolved over a long period of time (900 – 500 Ma) involving several episodes associated with subduction, magmatism and terrane accretion (Valeriano et al. 2008, Pimentel, 2016, Caxito et al. 2021, Heilbron et al., 2017, Campanha et al., 2023).

For the Brasília Belt in the West, closure of the Goiás-Pharusian ocean generated the major collisional event, constrained at ca. 630–600 Ma (Valeriano et al. 2008, Pimentel, 2016). Subsequent collisional and accretionary events followed in the Ribeira–Araçuaí belt at 585–530 Ma (Heilbron et al., 2017, Campanha et al., 2023), and the accretion of Cabo Frio Terrane in the Ribeira Belt at 530 –500 Ma (Schmitt et al. 2004, 2016). Collision of the Amazonian paleocontinent with closure of the Clymene ocean was proposed by Tohver et al. (2010) as occurred in early and middle Cambrian, generating the Araguaia-Paraguay-Pampean Orogen, with peak regional metamorphism at 496–484 Ma given by $^{40}Ar/^{39}Ar$ ages in illite.

For the Araçuaí Belt, several authors (e.g., Queiroga et al, 2016; Peixoto et al. 2018) point for a collisional stage at ca. 575-565 Ma, followed by a gravitational and extensional collapse stage from 530 to 490 Ma.

The new illite geochronological data from the southern São Francisco Craton marginal foreland covers suggest, however, that this period from 550 to 430 Ma represents a typical compressional fold-and-thrust belt regime, with thin-skinned tectonics and a double vergence towards the craton interior. The best interpretation is that in this post- or late-collisional period the neighbouring orogenic mountain building causes a compressional push toward the foreland region, in a Coulomb wedge driven model (Davis et al., 1983; Dahlen et al. 1984; Dahlen, 1990).

In marginal foreland fold-and-thrust belts, the Coulomb wedge model provides insights into how orogenic wedges grow and deform over time. These belts form in the foreland (outer regions) of an orogen, where tectonic compression causes the crust to shorten, often through a series of thrust faults and associated folds.

In the Coulomb wedge model, the stability and behaviour of the wedge are defined by its critical taper (θc) - the angle between the slope of the topographic surface (α) and the basal detachment slope (β) - that the wedge adopts to maintain a state of mechanical equilibrium (Fig.14). This taper angle is influenced by several factors, the most important being gravity, the internal

cohesion and friction of the material in the wedge, the strength of the basal detachment layer and the applied external (tectonic) forces.

The wedge can become over-steepened if compressional forces are too strong, causing the surface slope to exceed the critical taper. When the wedge reaches the critical taper, the next increment in deformation causes the basal detachment to propagate into the foreland, restoring a lower taper condition where internal deformation causes thickening with development or formation of new thrusts, folds, duplexes and shear zones. The wedge can become over steepened if compressional forces are too strong, causing the surface slope to exceed the critical taper. When this happens, gravity-driven collapse occurs, leading to extensional sliding complementing the otherwise compressional mechanism.

The Coulomb wedge model provides a robust model for understanding the development of the Neoproterozoic to Cambrian foreland fold-and-thrust belts along the margins of the São Francisco Craton. The critical taper, basal friction, and external forces shaping these belts during the Brasiliano Orogeny are consistent with the principles of wedge mechanics, where tectonic convergence drives the formation and growth of the fold-and-thrust belts. This model helps explain the geometry, structural styles, and dynamic evolution of these ancient orogenic systems.

Fig. 14. Application of the Coulomb wedge model to the marginal fold-and-thrust belts of the São Francisco Craton. (a) Schematic, not-to-scale cross-section of the central-southern São Francisco Craton (SFC - São Francisco Craton): Bftb – Brasília belt; Aftb – Araçuaí belt. Key: (1) eroded orogen surface; (2) present-day topographic surface; (3) Bambuí Group; (4) Macaúbas Group and equivalents; (5) Espinhaço Supergroup and equivalents; (6) higher metamorphic internal zones of the orogens; (7) São Francisco Craton basement. (b) Diagram illustrating the geometry of a critical wedge, where θc is the critical wedge angle, α represents the topographic slope, and β denotes the basal detachment (modified from McQuarrie and Ehlers, 2017).

Conclusions

This study focuses on the application of K-Ar illite dating aided by microstructural observations and detailed XRD characterization to constrain the timing and conditions of deformation in the Araçuaí and Brasília marginal fold-and-thrust belts, by analysing sedimentary covers of the São Francisco Craton from four distinct areas: Unaí, Curimataí-Buenópolis, Rodeador, and Serra do Cipó.

Our results indicate anchizonal temperature conditions compatible with previous estimates of ca. 250-270°C for deformation in the Unaí area (Brasília Belt, SW São Francisco Craton border). This is in contrast with the results from the SE São Francisco Craton border areas (Araçuaí Belt), where illite thermometry indicate significantly higher temperature conditions well within the Epizone, above with the K-Ar closure temperature range in illite, of ca. 350-250°C.

The analysis of different grain sizes showed that K-Ar ages in the finest fractions are generally younger than in coarser fractions, highlighting isotopic heterogeneity probably caused by the mixture of detrital illite and authigenic phases in the SW and protracted crystallization and/or grain-size dependent partial loss of radiogenic argon in the SE. This pattern suggests that detrital components significantly influence the isotopic system in the Unaí area, but set a maximum (older) estimate for deformation from 615 to 570 Ma at the São Francisco Craton western margin, while in the Curimataí-Buenópolis, Rodeador and Serra do Cipó areas, SE São Francisco Craton margin, K-Ar ages are related with the cooling history into upper crust temperature conditions following deformation at ca. 510 to 455 Ma.

These findings highlight the importance of late to post-collisional compression in shaping the foreland fold-and-thrust belts around the São Francisco Craton. The structural evolution of the fold-and-thrust belts is consistent with the Coulomb wedge model, in which tectonic compression from the Brasiliano Orogeny and the gravitational push of the neighbouring orogenic mountain building resulted in the development of oppositely-verging thin-skinned thrust systems. This model explains the observed deformation patterns and provides a framework for understanding the late-stage evolution of the São Francisco cratonic margins.

Acknowledgements

The authors would like to thank Professor Yildirim Dilekfor guidance in the editorial process, as well professor Amarildo Salina Ruiz, and an anonymous referee for comments and suggestions. GACC acknowledges the funding by FAPESP (2019/25599-9). GACC and FMF also thank CNPq for grants 304188/2022-0 and 310335/2022-1.

Author contributions

G.A.C.C. - Conceptualization, Investigation, Writing – Original Draft, Writing – Review & Editing, Visualization, Project Administration, Funding acquisition. **M. H.** - Methodology, Formal Analysis, Writing – Original Draft, Writing – Review & Editing, Visualization. **K.W.** - Methodology, Formal

Analysis, Resources, Writing – Original Draft, Writing – Review & Editing. **M.C.B.E.** - Investigation, Writing – Original Draft, Writing – Review & Editing, Visualization. **H.C.J.** - Investigation, Writing – Original Draft, Writing – Review & Editing, Visualization. **F.M.F.** - Investigation, Writing – Review & Editing. **R.S.S.V.** - Investigation, Writing – Review & Editing.

Funding information

This work was supported by FAPESP - Fundação de Amparo à Pesquisa do Estado de São Paulo (grant 2019/25599-9).

References

Alkmim, F.F., and Martins-Neto, M.A., 2001. A bacia intracratônica do São Francisco: arcabouço estrutural e cenários evolutivos. In: Pinto, C.P. and Martins-Neto, M.A. eds., *Bacia do São Francisco - Geologia e recursos naturais*, Belo Horizonte, SBG-MG, p. 9–30.

Alkmim, F.F., Brito-Neves, B.B., and Alves, J.A.C., 1993. *Arcabouço tectônico do Cráton do São Francisco: uma revisão* (J. M. Dominguez & A. Misi, Eds.): Salvador, SBG-BA/SBG-SE/SGM/CNPq, 45–62 p.

Alkmim, F. F.; Chemale Jr, F. ; Endo, I.1996. A deformação das coberturas proterozóicas do Cráton do São Francisco. *Revista da Escola de Minas*, Ouro Preto, v. 48, n.1, p. 14-31.

Alkmim, F.F., 2004. O que faz de um cráton um cráton? O Cráton do São Francisco e as revelações almeidianas ao delimitá-lo. In: Mantesso-Neto, V., Bartorelli, A., Carneiro, C.D.R., and Brito-Neves, B.B. eds., *Geologia do continente sul-americano: evolução da obra de Fernando Flávio Marques de Almeida*, São Paulo, Beca, p. 17–35.

Alkmim, F.F., Marshak, S., Pedrosa-Soares, A.C., Peres, G.G., Cruz, S.C.P., and Whittington, A., 2006. Kinematic evolution of the Araçuaí-West Congo Orogen in Brazil and Africa: nutcracker tectonics during the Neoproterozoic assembly of Gondwana. *Precambrian Research*, v. 149, p. 43–64, doi:10.1016/j.precamres.2006.06.007.

Almeida-Abreu, P. A., Renger, F. E. 2002. Serra do Espinhaço Meridional: Um Orógeno De Colisão Do Mesoproterozóico. *Revista Brasileira de Geociências*, 32(1), 01–14. https://doi.org/10.25249/0375-7536.20023210114

Almeida, F. F. M. 1967. *Origem e evolução da Plataforma Brasileira. Boletim*. Divisão de Geologia e Mineralogia. Rio de Janeiro: DNPM, n. 241, p. 1-36.

Almeida, F. F. M., & de Almeida, F. F. M. 1977. O Craton do São Francisco. *Revista Brasileira de Geociências*, *7*, 349–364. https://doi.org/10.5327/rbg.v7i4.128

Araújo, A. L. B., Barbosa, D. M. D., Rosa, P. A. S., & Roncato, J. 2020. Caracterização geológica-estrutural da conexão Araçuaí—São Francisco na área-tipo da Formação Rio Pardo Grande (Supergrupo Espinhaço, Minas Gerais). *Geonomos*. https://doi.org/10.18285/geonomos.v28i1.29652

Ault, A. K., Gautheron, C., King, G. E., 2019. Innovations in (U–Th)/He, fission track, and trapped charge thermochronometry with applications to earthquakes, weathering, surface-mantle connections, and the growth and decay of mountains. *Tectonics* 38(11), 3705-3739.

Babinski, M., Vieira, L. C., & Trindade, R. I. F. 2007. Direct dating of the Sete Lagoas cap carbonate (Bambuí Group, Brazil) and implications for the Neoproterozoic glacial events. *Terra Nova*, *19*(6), 401–406. https://doi.org/10.1111/j.1365-3121.2007.00764.x

Baptista. M. C.; Freitas, F.M.; Ribeiro, J.H.; Féboli, W.L.; Signorelli, N. 2015. *Carta Geológica Folha SE.23.V.A.III-Unaí Escala 1:100.000.* CPRM Serviço Geológico do Brasil.

Boles, A., Schleicher, A. M., Solum, J., van der Pluijm, B. 2018. Quantitative X-ray powder diffraction and the illite polytype analysis method for direct fault rock dating: A comparison of analytical techniques. *Clays and Clay Minerals* 66(3), 220-232.

Bosse, V., Villa, I. M., 2019. Petrochronology and hygrochronology of tectono-metamorphic events. *Gondwana Research* 71, 76-90.

Brito Neves, B.B., Kawashita, K., Delhal, J., 1979. Evolução geocronológica da cordilheira do Espinhaço;dados novos e integração. Revista Brasileira de Geociências 9, 71–85.

Campanha, G. A. C., Faleiros, F. M., Cabrita, D. I. G., Ribeiro, B. V., & Cawood, P. A. 2023. The southern Ribeira Belt in Western Gondwana: A record of a long-lived continental margin and terrane collage. *Journal of South American Earth Sciences*, *127*, 104404. https://doi.org/10.1016/j.jsames.2023.104404

Campos, J. E. G., Dardenne, M. A. 1997. Origem E Evolução Tectônica Da Bacia Sanfranciscana. *Revista Brasileira de Geociências*, 27(3), 283–264. https://doi.org/10.25249/0375-7536.1997283294

Caxito, F., Lana, C., Frei, R., Uhlein, G. J., Sial, A. N., Dantas, E. L., Pinto, A. G., Campos, F. C., Galvão, P., Warren, L. v., Okubo, J., & Ganade, C. E. 2021. Goldilocks at the dawn of complex life: mountains might have damaged Ediacaran–Cambrian ecosystems and prompted an early Cambrian greenhouse world. *Scientific Reports 2021 11:1*, *11*(1), 1–15. https://doi.org/10.1038/s41598-021-99526-z

Chang, H.K., Miranda, F.P., Magalhães, L., and Alkmim, F.F., 1988, Considerações sobre a evolução tectônica da Bacia do São Francisco. In: XXXV Congresso Brasileiro de Geologia, Belém, *Anais*, p. 2076–2090.

Chemale, F., Dussin, I.A., Alkmim, F.F., Martins, M.S., Queiroga, G., Armstrong, R., Santos, M.N., 2012. Unravelling a Proterozoic basin history through detrital zircon geochronology: The case of the Espinhaço Supergroup, Minas Gerais, Brazil. Gondwana Research 22, 200–206. https://doi.org/10.1016/j.gr.2011.08.016

Clauer, N, Chaudhuri, S., 1999. Isotopic dating of very low-grade metasedimentary and metavolcanic rocks: techniques and methods. In: Frey, M., Robinson, D. (Eds.), *Low-grade metamorphism*. John Wiley & Sons, 202-226

Coelho, J. C. C., Martins-Neto, M. A., & Marinho, M. S. 2008. Estilos estruturais e evolução tectônica da porção mineira da bacia proterozóica do São Francisco. *Revista Brasileira de Geociências*, 38(2), 149–165. https://doi.org/10.25249/0375-7536.2008382s149165

Dahlen, F.A., Suppe, J., and Davis, D., 1984. Mechanics of Fold-and-Thrust Belts and Accretionary Wedges: Cohesive Coulomb Theory. *Journal of Geophysical Research*, v. 89, p. 10087–10101, doi:10.1029/JB089iB12p10087.

Dahlen, F.A., 1990, Critical taper model of fold-and-thrust belts and accretionary wedges: *Annual Review of Earth & Planetary Sciences*, v. 18, p. 55–99, doi:10.1146/annurev.ea.18.050190.000415.

Dardenne, M.A., 1978. Geologia do Grupo Bambuí no vale do Rio Paraná (Goiás). In: XXX Congresso Brasileiro de Geologia, Recife, SBG, *Anais*, v. 2, p. 611–621.

Davis, D., Suppe, J., & Dahlen, F. A. 1983. Mechanics of fold-and- thrust belts and accretionary wedges. *Journal of Geophysical Research*, 88(B2), 1153–1172. https://doi.org/10.1029/JB088iB02p01153

Doebelin, N., Kleeberg, R., 2015. Profex: a graphical user interface for the Rietveld refinement program BGMN. *Journal of applied crystallography* 48(5), 1573-1580.

Duvall, A. R., Clark, M. K., van der Pluijm, B. A., Li, C., 2011. Direct dating of Eocene reverse faulting in northeastern Tibet using Ar-dating of fault clays and low-temperature thermochronometry. *Earth and Planetary Science Letters* 304(3-4), 520-526.

Engi, M., Lanari, P., Kohn, M. J., 2017. Significant ages—An introduction to petrochronology. *Reviews in Mineralogy and Geochemistry* 83(1), 1-12.

Esteves, M. C. B., & Faleiros, F. M. (2021). Fluid flow and syntectonic veining in an Ediacaran foreland fold-thrust zone, western margin of the São Francisco Craton, Brazil. *Journal of the Geological Society*, jgs2020-061. https://doi.org/10.1144/jgs2020-061

Fitz-Diaz, E., van der Pluijm, B., 2013. Fold dating: A new Ar/Ar illite dating application to constrain the age of deformation in shallow crustal rocks. *Journal of Structural Geology* , 54, 174-179.

Fogaça, A. C. C. 1997. *Geologia da Folha Diamantina*. In: GROSSI-SAD, J. H.; LOBATO, L. M.; PEDROSA-SOARES, A. C. & SOARES-FILHO, B. S. (coordenadores e editores). PROJETO ESPINHAÇO EM CD-ROM (textos, mapas e anexos). Belo Horizonte, COMIG - Companhia Mineradora de Minas Gerais. p. 1575-1665.

Fossen, H., Cavalcante, G. C. G., Pinheiro, R. V. L., Archanjo, C. J., 2019. Deformation–progressive or multiphase? *Journal of Structural Geology* 125, 82-99.

Fuck, R.A., Brito Neves, B.B., Schobbenhaus, C., 2008. Rodinia descendants in South America. Precambrian Research 160, 108–126. https://doi.org/10.1016/j.precamres.2007.04.018

Garduño-Martínez, D. E., Pi Puig, T., Solé, J., Martini, M., Alcalá-Martínez, J. R., 2015. K-Ar illite-mica age constraints on the formation and reactivation history of the El Doctor fault zone, central Mexico. *Revista mexicana de ciencias geológicas*, 32(2), 306-322.

Gautheron, C., Hueck, M., Ternois, S., Heller, B., Schwartz, S., Sarda, P., Tassan-Got, L., 2022. Investigating the Shallow to Mid-Depth (> 100–300° C) Continental Crust Evolution with (U-Th)/He Thermochronology: A Review. *Minerals* 12(5), 563.

Grathoff, G.H., Moore, D.M., 1996. Illite polytype quantification using Wildfire calculated x-ray diffraction patterns. *Clays and Clay Minerals* 44(6), 835-842.

Grathoff, G.H., Moore, D.M., Hay, R.L., Wemmer, K., 2001. Origin of illite in the lower Paleozoic of the Illinois basin: Evidence for brine migrations. *Geological Society of America Bulletin* 113, 1092–1104.

Harrison, T.M., Célérier, J., Aikman, A.B., Hermann, J., Heizler, M.T., 2009. Diffusion of 40Ar in muscovite. *Geochimica et Cosmochimica Acta* 73, 1039-1051.

Heilbron, M., Cordani, U. G., & Alkmim, F. F. (2017). *São Francisco Craton, Eastern Brazil: Tectonic Genealogy of a Miniature Continent*. Springer. https://doi.org/10.1007/978-3-319-01715-0

Hower, J. O. H. N., Hurley, P. M., Pinson, W. H., Fairbairn, H. W., 1963. The dependence of K-Ar age on the mineralogy of various particle size ranges in a shale. *Geochimica et Cosmochimica acta* 27(5), 405-410.

Hueck, M., Oriolo, S., Dunkl, I., Wemmer, K., Oyhantçabal, P., Schanofski, M., Basei, M.A.S., Siegesmund, S., 2017. Phanerozoic low-temperature evolution of the Uruguayan Shield along the South American passive margin. J*ournal of the Geological Society* 174, 609-626.

Hueck, M., Wemmer, K., Basei, M. A., Philipp, R. P., Oriolo, S., Heidelbach, F., Oyhantçabal, P., Siegesmund, S. 2020. Dating recurrent shear zone activity and the transition from ductile to

brittle deformation: White mica geochronology applied to the Neoproterozoic Dom Feliciano Belt in South Brazil. *Journal of Structural Geology* 141, 104199.

Hueck, M., Wemmer, K., Ksienzyk, A., Kuehn, R., Vogel, N., 2022. Potential, premises, and pitfalls of interpreting illite argon dates - a case study from the German Variscides. *Earth Science Reviews*, 104133

Hunziker, J.C., Frey, M., Clauer, N., Dallmeyer, R.D., Friedrichsen, H., Flehmig, W., Hochstrasser, K., Roggwiler, P., Schwander, H., 1986. The evolution of illite to muscovite: mineralogical and isotopic data from the Glarus Alps, Switzerland. *Contributions to Mineralogy and Petrology* 92(2), 157-180.

Joncew, H. C. (2024). *Tectonic evolution of the Southern Espinhaço Front in Serra do Cipó-MG*. Tese de Doutorado, Instituto de Geociências, Universidade de São Paulo, São Paulo. doi:10.11606/T.44.2024.tde-20062024-092228.

Joncew, H. C., & Campanha, G. A. da C. (2025). The Espinhaço Supergroup at the craton-orogen transition in Serra do Cipó-Brazil: Multi-statistical analyses of new and compiled detrital zircon U-Pb ages. *Journal of South American Earth Sciences*, *157*, 105422. https://doi.org/10.1016/j.jsames.2025.105422

Kirschner, D. L., Cosca, M. A., Masson, H., Hunziker, J. C., 1996. Staircase 40/Ar39Ar spectra of fine-grained white mica: Timing and duration of deformation and empirical constraints on argon diffusion. *Geology* 24(8), 747-750.

Knauer, L. G. et al. 2011. *Mapa geológico Folha Corinto - SE.23-Z-A-II escala 1:100.000*. CPRM.

Knauer, L. G. et al. 2014. *Geologia e recursos minerais da folha Corinto SE.23-Z-A-II : Estado de Minas Gerais*. Belo Horizonte : CPRM, 2014. 68 p. : il.; 30 cm ISBN 978-85-7499-214-3.

Köster, J. 1984. *Geologie der Nordwestlichen Serra Mineira südöstlich Von Buenópolis (Proterozoikum, Serra do Espinhaço, Minas Gerais, Brasilien)*. Universidade de Freiburg, Diplomarbeit, 85 p.

Ksienzyk, A.K., Wemmer, K., Jacobs, J., Fossen, H., Schomberg, A.C., Süssenberger, A., Lünsdorf, N.K., Bastesen, E., 2016. Post-Caledonian brittle deformation in the Bergen area,West Norway: results from K–Ar illite fault gouge dating. *Norwegian Journal of Geology* 96 (3), 1-25.

Kübler, B., 1967. *La cristallinité de l´illite et les zones tout à fait supérieures du métamorphism. Etages Tectonique*, Colloque de Neuchâtel, Neuchâtel.

Kuchenbecker, M., Pedrosa-Soares, A. C., Babinski, M., Reis, H. L. S., Atman, D., & Costa, R. D. da. 2020. Towards an integrated tectonic model for the interaction between the Bambuí basin and the adjoining orogenic belts: Evidences from the detrital zircon record of syn-orogenic units. *Journal of South American Earth Sciences*, 104, 102831. https://doi.org/10.1016/j.jsames.2020.102831

Löbens, S., Bense, F.A., Wemmer, K., Dunkl, I., Costa, C.H., Layer, P., Siegesmund, S., 2011. Exhumation and uplift of the Sierras Pampeanas: preliminary implications from K-Ar fault gouge dating and low-T thermochronology in the Sierra de Comechingones (Argentina). International J*ournal of Earth Sciences* 100, 671–694.

Lopes, T.C., 2012. O Supergrupo Espinhaço na Serra do Cabral, Minas Gerais: contribuição ao estudo de proveniência sedimentar. PhD thesis, UFMG. http://www.bibliotecadigital.ufmg.br/dspace/handle/1843/LGSA-97RNCY

Machado, N., Schrank, A., Abreu, F. R., Knauer, L. G., Almeida-Abreu, P.A., 1989. Resultados preliminares da geocronologia U-Pb na Serra do Espinhaço Meridional. Boletim do Núcleo Minas Gerais, n.10 171–174.

Martins, M.S et al. 2011. *Mapa Geológico Folha Serra do Cabral - SE.23-X-C-V escala 1:100.000.* CODEMIG, UFMG e CPRM.

Martins-Ferreira, M. A. C. 2019. Effects of initial rift inversion over fold-and-thrust development in a cratonic far-foreland setting. *Tectonophysics*, 757(October 2018), 88–107. https://doi.org/10.1016/j.tecto.2019.03.009

Martins-Neto, M. A., A. C. Pedrosa-Soares, e S. A.A. Lima. 2001. Tectono-sedimentary evolution of sedimentary basins from Late Paleoproterozoic to Late Neoproterozoic in the São Francisco craton and Araçuaí fold belt, Eastern Brazil. *Sedimentary Geology* 141–142:343–70. https://doi.org/10.1016/S0037-0738(01)00082-3.

McDougall, I., Harrison, T. M., 1999. *Geochronology and Thermochronology by the 40Ar/39Ar Method*. Oxford University Press on Demand.

McQuarrie, N., & Ehlers, T. A. 2017. Techniques for understanding fold-and-thrust belt kinematics and thermal evolution. In: R. D. Law, J. R. Thigpen, A. J. Merschat, & H. H. Stowell (Orgs.), *Linkages and Feedbacks in Orogenic Systems* (Vol. 213, p. 0). Geological Society of America. https://doi.org/10.1130/2017.1213(02)

Medeiros, G., Martins, M., Queiroga, G., Dias, L., Ciarallo, F., Alkmim, F., Dussin, I., Lana, C., 2024. Tectonostratigraphic framework and provenance of a Mesoproterozoic rift succession: An example from the Espinhaço Supergroup, SE Brazil. Precambrian Research 413, 107576. https://doi.org/10.1016/j.precamres.2024.107576

Merriman, R.J., Frey, M., 1999. Patterns of very low-grade metamorphism in metapelitic rocks. Low-grade metamorphism. In Frey, M., Robinson, D. (Eds.), *Low-Grade Metamorphism*, Blackwell Science, Oxford, 61–107.Meunier, A., Velde, B., 2004. Illite: Origins, evolution and metamorphism. Springer Science & Business Media.

Meunier, A., Velde, B., 2004. I*llite: Origins, evolution and metamorphism*. Springer Science & Business Media.

Monié, P., Münch, P., Milesi, G., Bonno, M., Iemmolo, A., 2024. 40Ar/39Ar geochronology of crustal deformation. *Comptes Rendus. Géoscience* 356(S2), 495-524.

Moore, D. M., Reynolds, R. C. 1997. *X-ray Diffraction and the Identification and Analysis of Clay Minerals*. Oxford: Oxford university press, 2nd edition.

Mora, C. A. S., Campanha, G. A. da C., & Wemmer, K.,2013. Microstructures and K-Ar illite fine-fraction ages of the cataclastic rocks associated to the Camburu Shear Zone, Ribeira Belt, Southeastern Brazil. *Brazilian Journal of Geology*, 43(4), 607–622. https://doi.org/10.5327/Z2317-48892013000400003

Moraes, L. J. 1937. Geologia econômica do norte de Minas Gerais. Dep. Nac. Prod. Mineral, Serv. Fom. Prod. Mineral, Bol. 19, Rio de Janeiro. 192 p.

Moreira, D. S., Uhlein, A., Dussin, I. A., Uhlein, G. J., & Pimentel Misuzaki, A. M. 2020. A Cambrian age for the upper Bambuí Group, Brazil, supported by the first U-Pb dating of volcaniclastic bed. *Journal of South American Earth Sciences*, *99*(August 2019), 102503. https://doi.org/10.1016/j.jsames.2020.102503

Nierhoff, R., Clauer, N., Spaeth, G., 2011. New findings on the tectono-metamorphic history of the western Rhenish Massif (Germany) by K–Ar dating of metasedimentary illite. Journal of *Geodynamics* 52(2), 129-142.

Noce, C. M. 1997. Geologia da Folha Curimataí. In: GROSSI-SAD, J. H.; LOBATO, L. M.; PEDROSA-SOARES, A. C. & SOARES-FILHO, B. S. (coordenadores e editores). PROJETO ESPINHAÇO EM CD-ROM*(textos, mapas e anexos)*. Belo Horizonte, COMIG - Companhia Mineradora de Minas Gerais. p. 1199-1250.

Oriolo, S., Wemmer, K., Oyhantçabal, P., Fossen, H., Schulz, B., & Siegesmund, S., 2018. Geochronology of shear zones – A review. *Earth-Science Reviews* 185, 665-683.

Oriolo, S., Schulz, B., Hueck, M., Oyhantcabal, P., Heidelbach, F., Sosa, G., Siegesmund, S., 2022. The petrologic and petrochronologic record of progressive vs polyphase deformation: Opening the analytical toolbox. *Earth-Science Reviews*, 104235.

Parry, W. T., Bunds, M. P., Bruhn, R. L., Hall, C. M., Murphy, J. M., 2001. Mineralogy, 40Ar/39Ar dating and apatite fission track dating of rocks along the Castle Mountain fault, Alaska. *Tectonophysics* 337(3-4), 149-172.

Paula-Santos, G.M.; Caetano-Filho, S.; Babinski, M.; Trindade, R.I.F.; Guacaneme, C. 2017. Tracking connection and restriction of West Gondwana São Francisco Basin through isotope chemostratigraphy. *Gondwana Research*, 42: 280-305.

Paula-Santos, G. M., Babinski, M., Kuchenbecker, M., Caetano-Filho, S., Trindade, R. I., & Pedrosa-Soares, A. C. (2015). New evidence of an Ediacaran age for the Bambuí Group in southern São Francisco craton (eastern Brazil) from zircon U–Pb data and isotope

chemostratigraphy. *Gondwana Research*, 28(2), 702–720. https://doi.org/10.1016/j.gr.2014.07.012

Pedrosa-Soares, A.C., and Alkmim, F.F., 2011, How many rifting events preceded the development of the Araçuaí-West Congo Orogen? *Geonomos*, v. 19, p. 244–251.

Pedrosa-Soares, A. C., Noce, C. M., Vidal, P., Monteiro, R. L. B. P., & Leonardos, O. H. (1992). Toward a new tectonic model for the Late Proterozoic Araçuaí (SE Brazil)-West Congolian (SW Africa) Belt. *Journal of South American Earth Sciences*, 6(1–2), 33–47. https://doi.org/10.1016/0895-9811(92)90015-Q

Pedrosa-Soares, A.C., Vidal, P., Leonardos, O.H., and Brito-Neves, B.B., 1998, Neoproterozoic oceanic remnants in eastern Brazil: further evidence and refutation of an exclusively ensialic evolution for the Araçuaí-West Congo Orogen. *Geology*, v. 26, p. 519–522, doi:10.1130/0091-7613(1998)026<0519:NORIEB>2.3.CO;2.

Pedrosa-Soares, A. C., Noce, C. M., Wiedemann, C. M., & Pinto, C. P. (2001). The Araçuaí-West-Congo Orogen in Brazil: An overview of a confined orogen formed during Gondwanaland assembly. *Precambrian Research*, 110(1–4), 307–323. https://doi.org/10.1016/S0301-9268(01)00174-7

Pedrosa-Soares, A. C. ; Noce, C. M. ; Alkmim, F. F.; Silva, L. C. ; Babinski, M. ; Cordani, U.G. ; Castañeda, C,. Orógeno Araçuaí: SÍNTESE DO CONHECIMENTO 30 ANOS APÓS Almeida 1977. 2007. *Geonomos*, v. 15, p. 1-16, 2007.

Peixoto, E., Alkmim, F. F., Pedrosa-Soares, A., Lana, C., & Chaves, A. O. (2018). Metamorphic record of collision and collapse in the Ediacaran-Cambrian Araçuaí orogen, SE-Brazil: Insights from P–T pseudosections and monazite dating. *Journal of Metamorphic Geology*, 36(2), 147–172. https://doi.org/10.1111/jmg.12287

Pimentel, M. M. (2016). The tectonic evolution of the Neoproterozoic Brasília Belt, central Brazil: A geochronological and isotopic approach. *Brazilian Journal of Geology*, 46(June), 67–82. https://doi.org/10.1590/2317-4889201620150004

Pimentel, M.M.; Rodrigues, J.B.; DellaGiustina, M.E.S.; Junges, S.; Matteini, M.; Armstrong, R. 2011. The tectonic evolution of the Neoproterozoic Brasília Belt, central Brazil, based on SHRIMP and LA-ICP-MS U-Pb sedimentary provenance data: A review. *Journal of South American Earth Sciences*., 31: 345-357.

Queiroga, G. N., Schulz, B., Martins, M. de S., Castro, M. P. de, Pedrosa-Soares, A. C., Jordt-Evangelista, H., & Silva, A. L. da. (2016). Thermobarometry and electron-microprobe Th-U-Pb monazite dating in garnet metapelites from the Capelinha Formation, Araçuaí Orogen, Brazil. Rem: *Revista Escola de Minas*, 69, 33–44. https://doi.org/10.1590/0370-44672015690066

Rahl, J. M., Haines, S. H., van der Pluijm, B. A., 2011. Links between orogenic wedge deformation and erosional exhumation: Evidence from illite age analysis of fault rock and detrital thermochronology of syn-tectonic conglomerates in the Spanish Pyrenees. *Earth and Planetary Science Letters* 307(1-2), 180-190.

Reis, H. L. S., Suss, J. F., Fonseca, R. C. S., & Alkmim, F. F. (2017). Ediacaran forebulge grabens of the southern São Francisco basin, SE Brazil: Craton interior dynamics during West Gondwana assembly. *Precambrian Research*, 302(March), 150–170. https://doi.org/10.1016/j.precamres.2017.09.023

Reuter, A., Dallmeyer, R. D., 1989. K-Ar and 40Ar/39Ar dating of cleavage formed during very low-grade metamorphism: a review. *Geological Society of London Special Publications* 43(1), 161-171.

Roberts, N. M., Žák, J., Vacek, F., Sláma, J., 2021. No more blind dates with calcite: Fluid-flow vs. fault-slip along the Očkov thrust, Prague Basin. *Geoscience Frontiers* 12(4), 101143.

Rodrigues, J. B. 2008. *Proveniência de sedimentos dos grupos Canastra, Ibiá, Vazante e Bambuí : um estudo de zircões detríticos e idades modelo Sm-Nd*. PhD Thesis, UnB https://repositorio.unb.br/handle/10482/3581.

Queiroga, G.N., Dussin, I.A., Martins, M., Machado, M.C., Kawashita, K., Chemale, F., 2012. Roteiro de Campo – Rochas Ígneas. In: Dussin, I.A., Chemale, F. (Eds.), Geologia Estrutural e Estratigrafia do Sistema Espinhaço – Chapada Diamantina e sua Aplicação nas Bacias Mesocenozóicas da Margem Passiva Brasileira. FUNDEP/ PETROBRÁS, Belo Horizonte, pp. 170–195

Schomberg, A.C., Wemmer, K., Warr, L.N., Grathoff, G.H., 2019. K–Ar age determinations on the fine fractions of clay mineral 'Crystallinity Index Standards' from the Palaeozoic mudrocks of southwest England. *Clay Minerals* 54(1), 15-26.

Serviço Geológico do Brasil, 2025. Geologia do Brasil em 1:2.500.000. https://geosgb.sgb.gov.br/geosgb/downloads.html.

Silva Lara, H., Oyhantçabal, P., Wemmer, K., Hueck, M., Basei, M.A.S., Siegesmund, S., 2021. The Sierra de Aguirre Formation: Post-Collisional Ediacaran Volcanism in the Southernmost Dom Feliciano Belt. J*ournal of South American Earth Sciences* 103118

Süssenberger, A., De Brito Neves, B. B., & Wemmer, K. 2014. Dating low-grade metamorphism and deformation of the espinhaço supergroup in the Chapada Diamantina (Bahia, NE Brazil): A K/Ar fine-fraction study. Brazilian *Journal of Geology*, 44(2), 207–220. https://doi.org/10.5327/Z2317-4889201400020003

Souza, M.E.S. 2016. Caracterização litoestrutural e geocronológica dos xistos verdes e metagabros do Grupo Macaúbas nas regiões de Terra Branca e Planalto de Minas, Minas Gerais. MSc

thesis, Departamento de Geologia – Escola de Minas, Universidade Federal de Ouro Preto, 263p

Süssenberger, A., Schmidt, S. T., Wemmer, K., Baumgartner, L. P., Grobéty, B., 2018a. Timing and thermal evolution of fold-and-thrust belt formation in the Ultima Esperanza District, 51° S Chile: Constraints from K-Ar dating and illite characterization. *GSA Bulletin* 130(5-6), 975-998.

Süssenberger, A., Wemmer, K., Schmidt, S. T., 2018b. The zone of incipient 40Ar* loss - monitoring 40Ar* degassing behavior in a contact metamorphic setting. *Applied Clay Science* 165, 52-63.

Tavares, T. D., Martins, M. de S., Alkmim, F. F., & Lana, C. 2020. Detrital zircons from the Upper Três Marias Formation, São Francisco basin, SE Brazil: Record of foreland deposition during the Cambrian? *Journal of South American Earth Sciences*, 97(March 2019), 102395. https://doi.org/10.1016/j.jsames.2019.102395

Uhlein, G. J., Uhlein, A., Stevenson, R., Halverson, G.P., Caxito, F.A., Cox, G.M.. 2017. Early to late Ediacaran conglomeratic wedges from a complete foreland basin cycle in the southwest São Francisco Craton, Bambuí Group, Brazil. *Precambrian Research* 299, p.101–16. https://doi.org/10.1016/j.precamres.2017.07.020.

Valeriano, C. M., Pimentel, M. M., Heilbron, M., Almeida, J. C. H., & Trouw, R. A. J. 2008. Tectonic evolution of the Brasília Belt, Central Brazil, and early assembly of Gondwana. *Geological Society, London, Special Publications*, 294(1), 197–210. https://doi.org/10.1144/SP294.11

van der Pluijm, B.A., Hall, C.M., Vrolijk, P.J., Pevear, D.R., Covey, M.C., 2001. The dating of shallow faults in the Earth's crust. *Nature* 412(6843), 172.

Verdel, C., van der Pluijm, B. A., Niemi, N., 2012. Variation of illite/muscovite 40 Ar/39 Ar age spectra during progressive low-grade metamorphism: an example from the US Cordillera. *Contributions to Mineralogy and Petrology* 164(3), 521-536.

Viola, G., Scheiber, T., Fredin, O., Zwingmann, H., Margreth, A., Knies, J., 2016. Deconvoluting complex structural histories archived in brittle fault zones. *Nature communications* 7, 13448.

Warr, L. N., 1996. Standardized clay mineral crystallinity data from the very low-grade metamorphic facies rocks of southern New Zealand. *European Journal of Mineralogy* 8(1), 115-127.

Warr, L. N., Ferreiro-Mählmann, R. F., 2015. Recommendations for Kübler index standardization. *Clay Minerals* 50(3), 283-286.

Warr, L. N., 2018. A new collection of clay mineral 'Crystallinity'Index Standards and revised guidelines for the calibration of Kübler and Árkai indices. *Clay Minerals* 53(3), 339-350.

Warren, L.V.; Quaglio, F.; Riccomini, C.; Simões, M.G.; Poiré, D.G.; Strikis, N.M; Anelli, L.E; Strikis, P.C. 2014. The puzzle assembled: Ediacaran guide fossil Cloudina reveals an old proto-Gondwana seaway. *Geology*, 42: 391-394.

Wemmer, K., Ahrendt, H., 1997. Comparative K-Ar and Rb-Sr age determinations of retrograde processes on rocks from the KTB deep drilling project. *Geologische Rundschau* 86, S272.

Zwingmann, H., Yamada, K., Tagami, T., 2010. Timing of brittle deformation within the Nojima fault zone, Japan. *Chemical Geology*, 275(3-4), 176-185.

Table 1 – Samples context and units. ES- Espinhaço Supergroup; BG - Bambuí Group.

Sample	Lithology	Context	Unit	Latitude	Longitude
HJ 41	metasandstone (mylonitic)	Near Espinhaço main thrust	ES, Santa Rita F. (*)	-19.34	-43.6
HJ 98b	metasandstone	Near Espinhaço main thrust	ES, Santa Rita F. (*)	-19.28	-43.62
HJ 165	metapelite	Foreland, Araçuaí side	BG, S. Santa Helena F.	-19.25	-43.66
HJ 169	metapelite	Foreland, Araçuaí side	BG, S. Santa Helena F.	-19.28	-43.69
UN 04	siltstone	Foreland, Brasília side	Paranoá Group (**)	-16.21	-46.66
UN 14	siltstone	Foreland, Brasília side	BG, Paraopeba Subg.	-16.26	-46.81
UN 21b	siltstone	Foreland, Brasília side	BG, Paraopeba Subg.	-16.32	-46.88
N10	metasiltstone	Foreland, Araçuaí side	BG, S. Santa Helena F.	-17.85	-44.17
N24	metasiltstone	Top unit of the Espinhaço Sg.	ES, Rio Pardo Grande F.	-18.3	-44.01
N43A	metasiltstone	Foreland, Araçuaí side	BG, S. Santa Helena F.	-17.94	-44.06
N49	metasiltstone	Near Espinhaço / Macaúbas unconformity	ES, Santa Rita F.	-17.99	-43.99

(*) In some previous works as Macaúbas Group. (**) In some previous works as Bambuí Group.

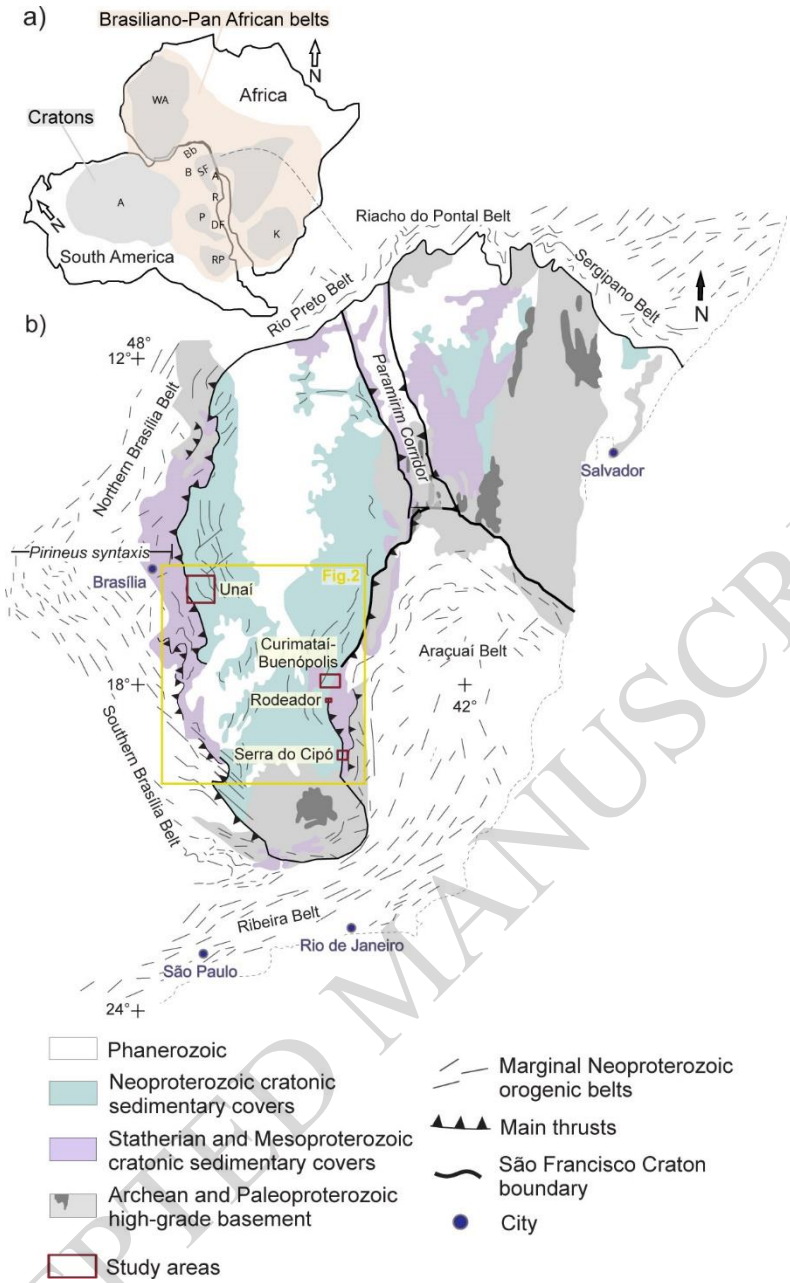

Figure 1

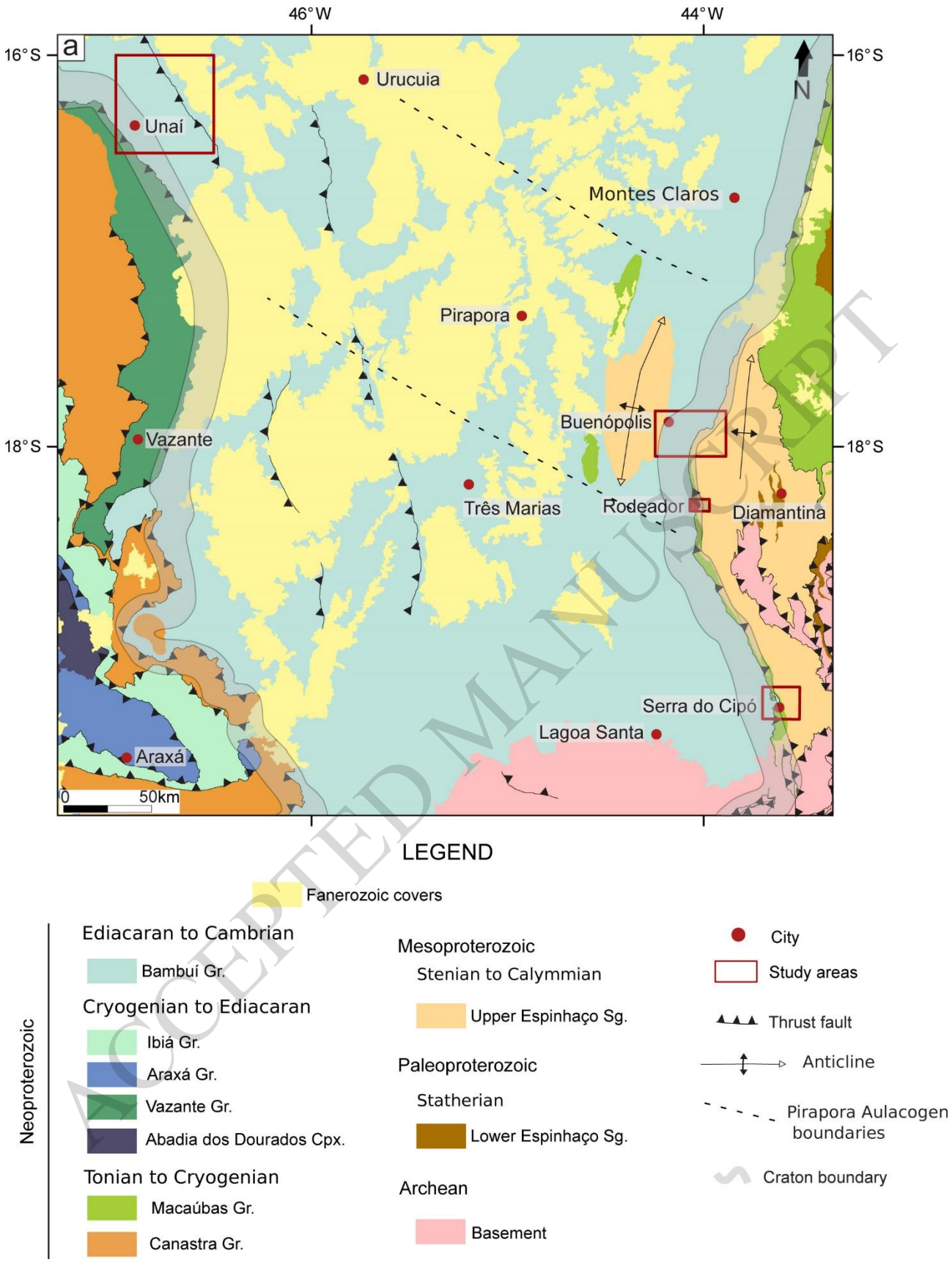

Figure 2

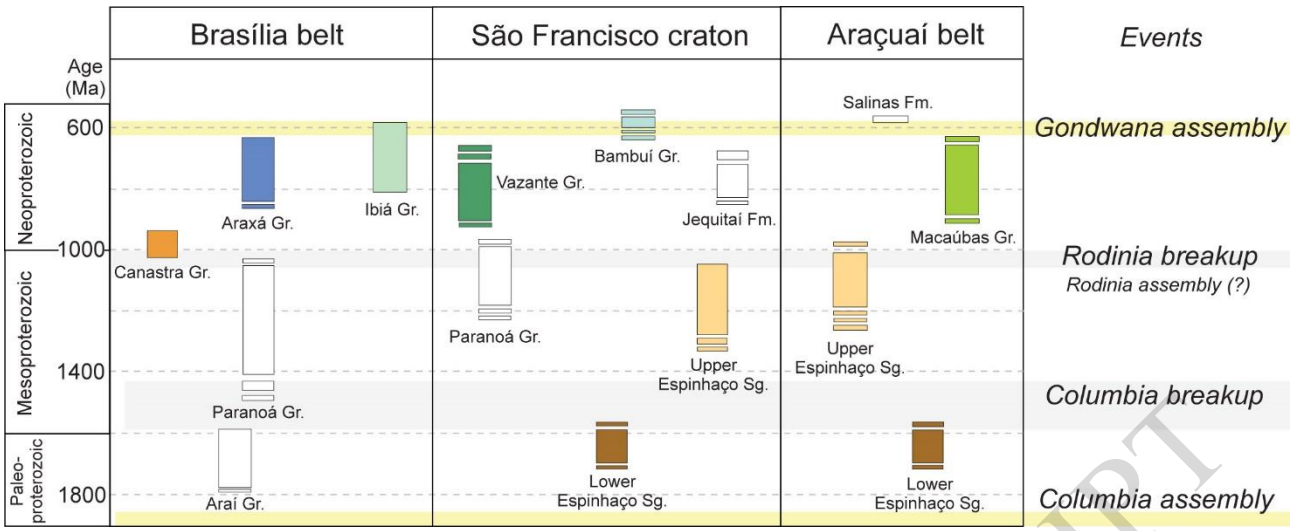

Figure 3

Supergroup		Group	Formation		Unconformity	Age (Ma) YZG	Age (Ma) Other	Basin Type	Depositional Environment
São Francisco		Bambuí	Três Marias			527 ± 4 [1] 543 ± 9 [2] 616 [3]		foreland basin	shallow marine
			Paraopeba Subgroup	Serra da Saudade		520.2 ± 5.3 [4] 513 ± 6 [2]			
				Lagoa do Jacaré					
				Serra de Sta Helena		543±9 [2] 612 [3]			
				Sete Lagoas		557 [5] 609 [3]	740 ± 22 [8] 550 and 542 [9]		
		Macaúbas	undivided	Jequitaí		860+31 [3]	Pedro Lessa mafic Suite 906 ±2 [10] 933± 20 [11] 939± 7 [12]	rift	alluvial, aeolian
					angular				
Espinhaço	Upper	Conselheiro Mata	Rio Pardo Grande			1445± 25 [6]		sag basin	shallow marine
			Córrego Pereira			1329± 12 [6]			
			Córrego Bandeira						
			Córrego dos Borges			1379 ± 15 [6] 1400 [7]			
			Santa Rita		paraconformity	1487 ± 40 [6] 1400 [7]			
			Galho do Miguel		paraconformity	1862 ± 16 [6] 1300 [7]			aeolian
			Sopa-Brumadinho		angular	1080 ± 16 [6]		rift	lacustrine, fan delta
	Lower		São João da Chapada		angular	1703 ± 12 [6]	Conceição do Mato Dentro Suite 1711+4 [10] 1770 [13]	rift	lacustrine, alluvial, braidplain
			Bandeirinha			1709 ± 10			alluvial, aeolian
undivided basement									

Figure 4

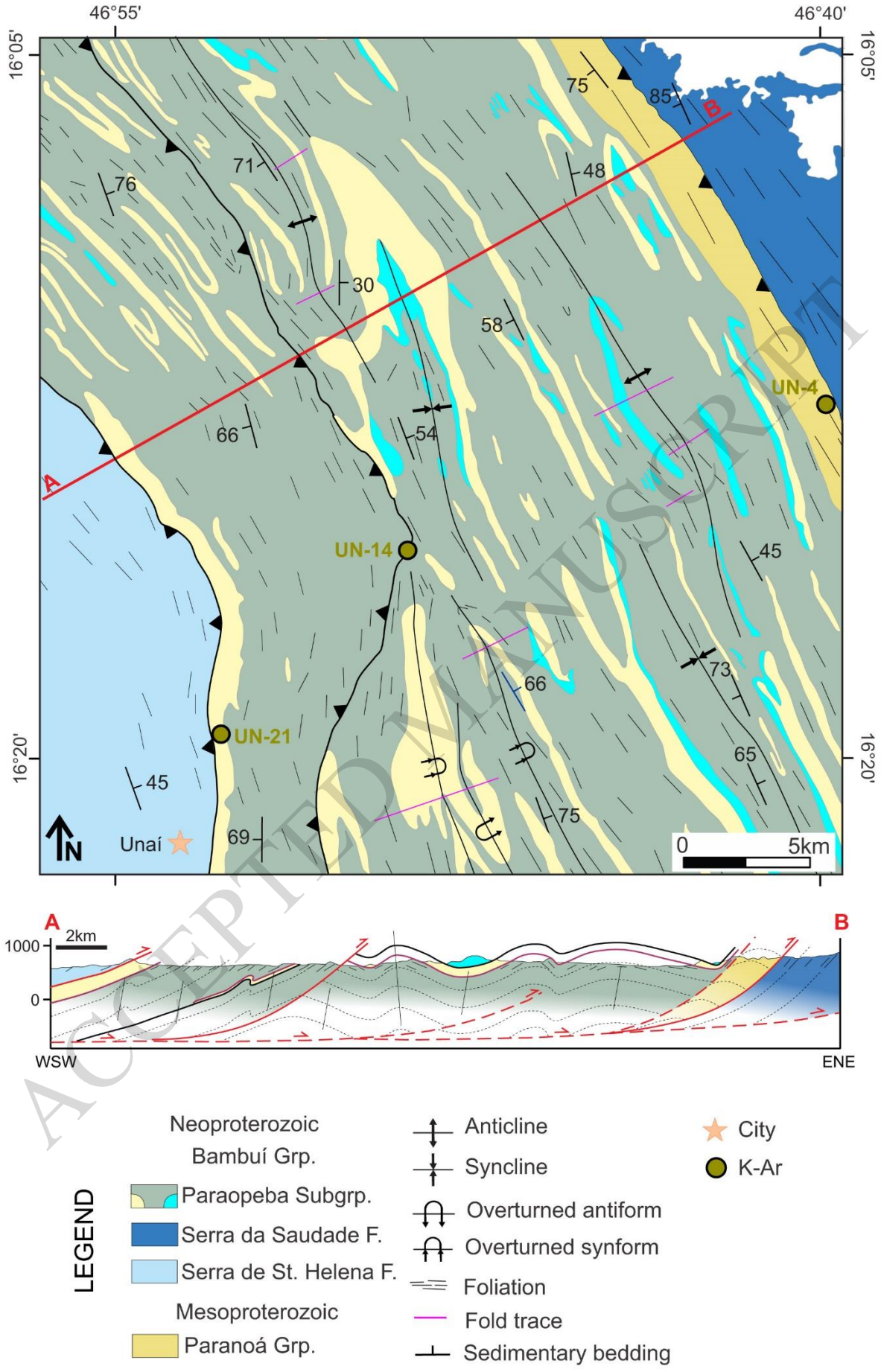

Figure 5

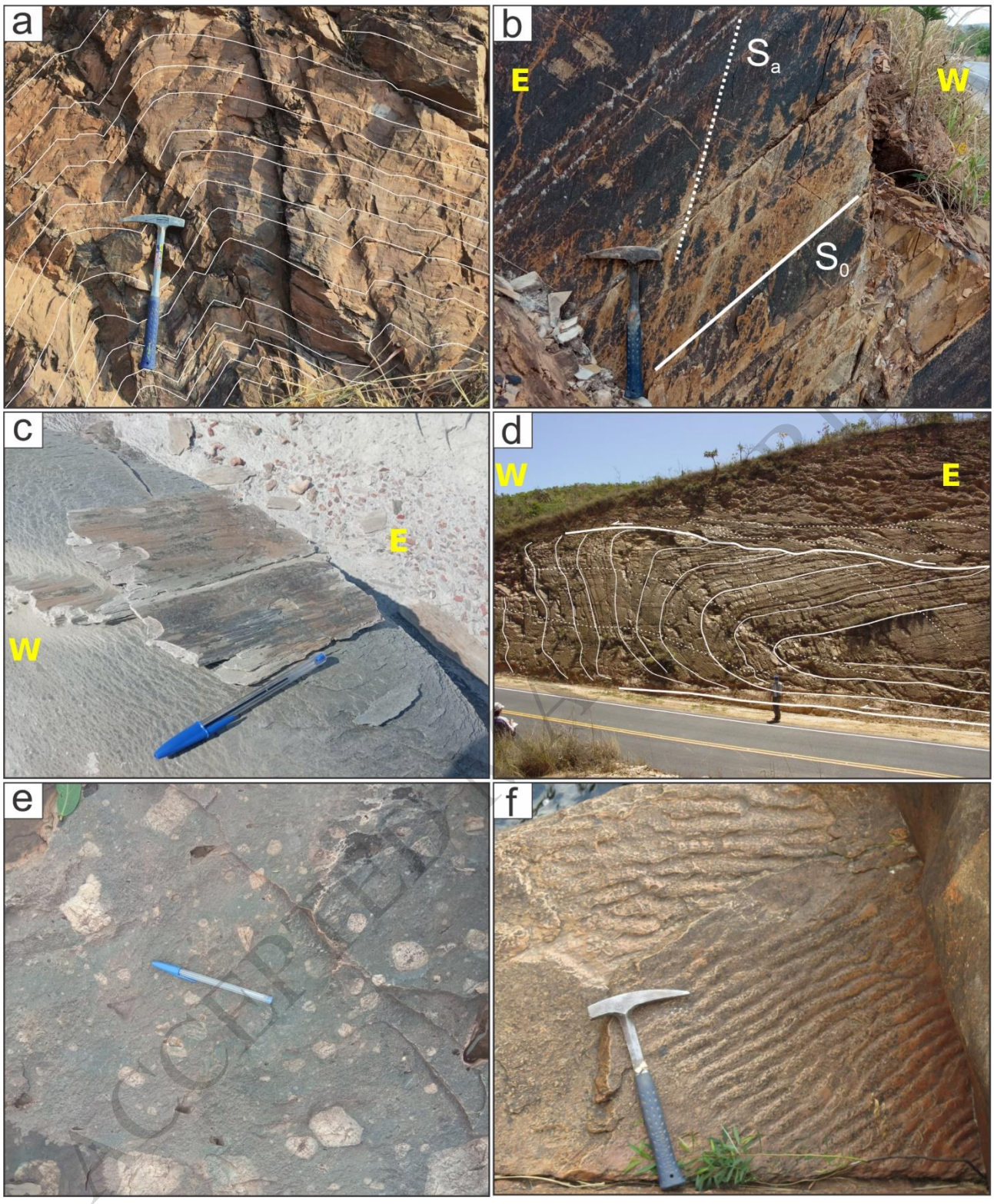

Figure 6

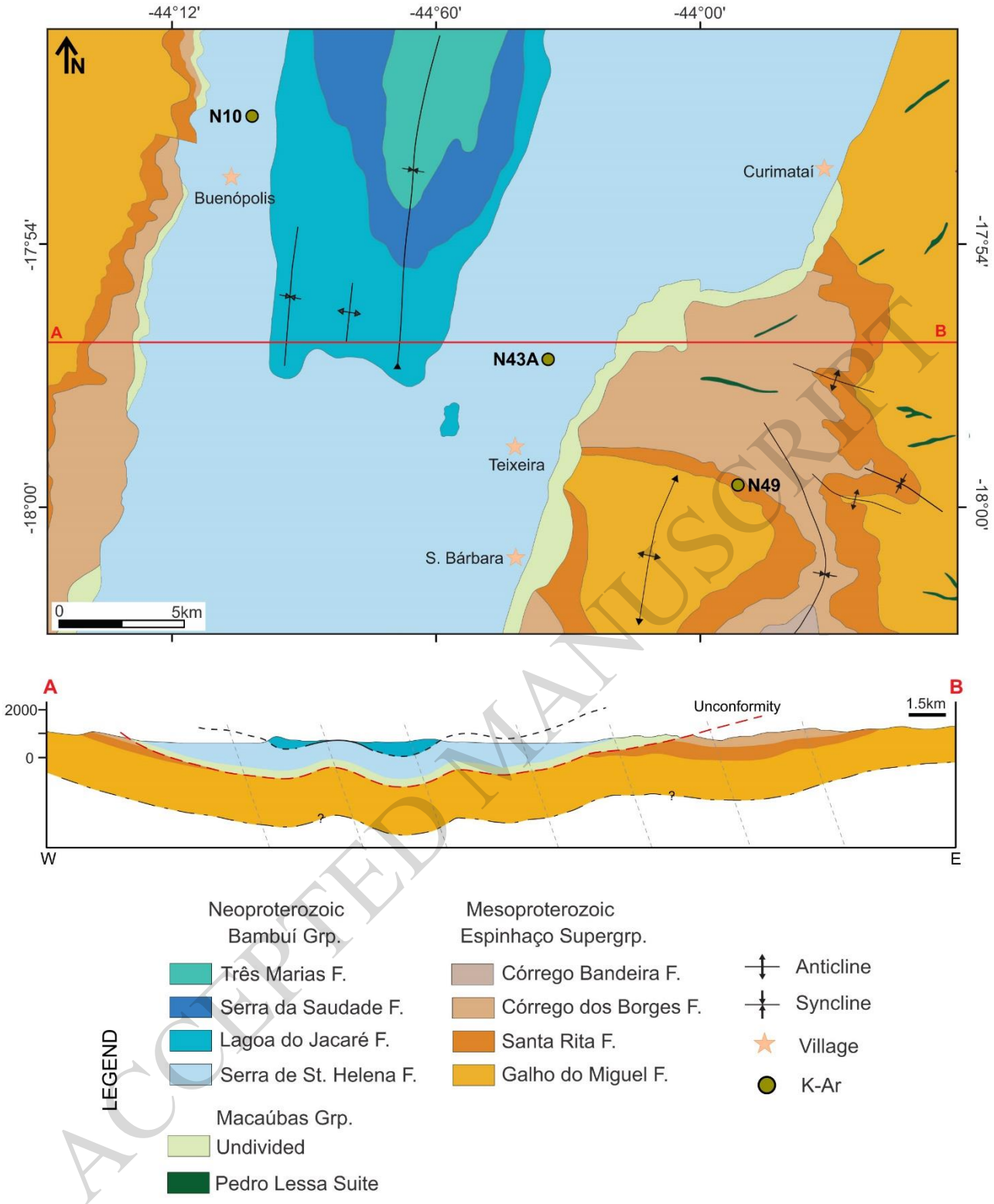

Figure 7

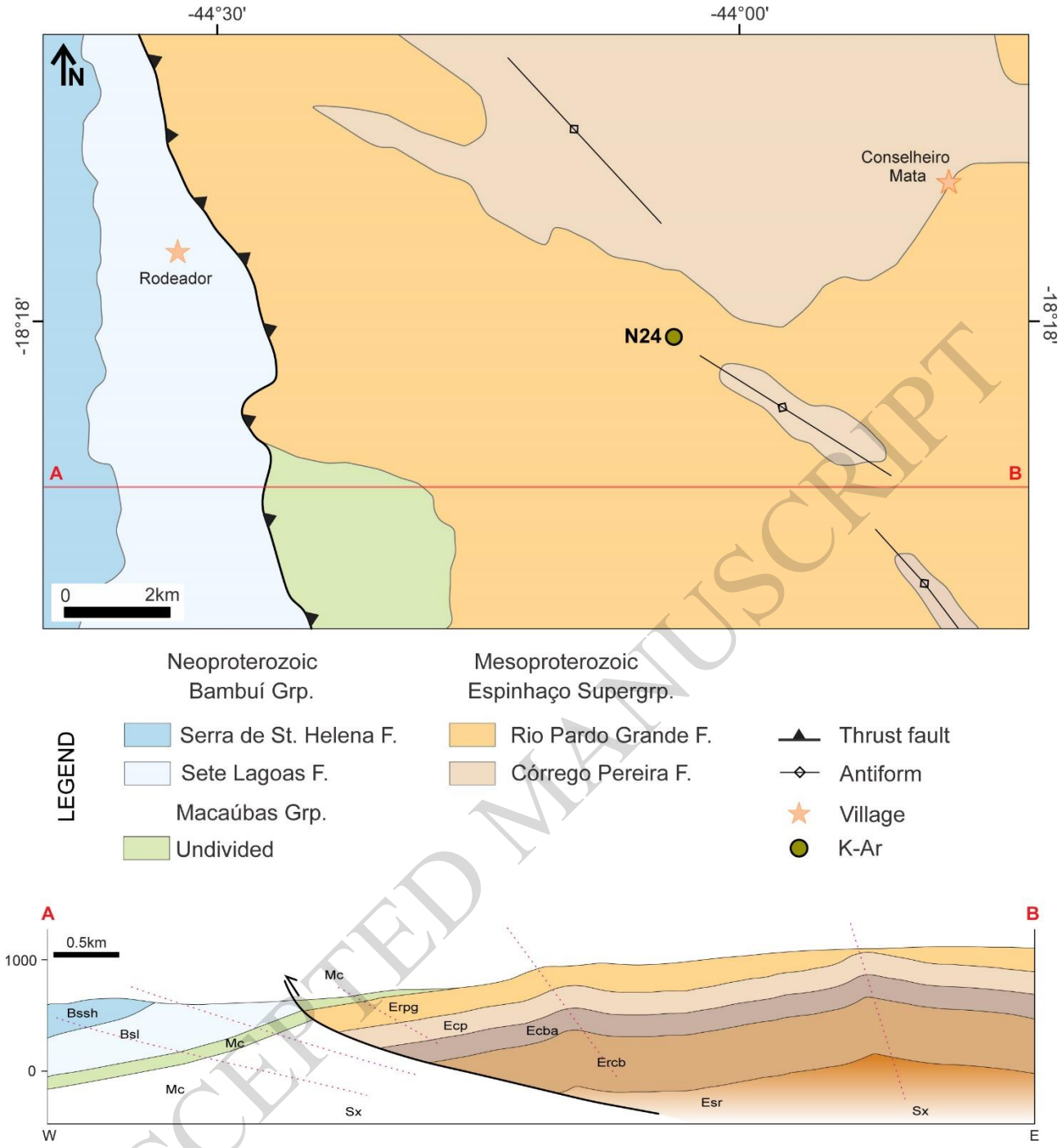

Figure 8

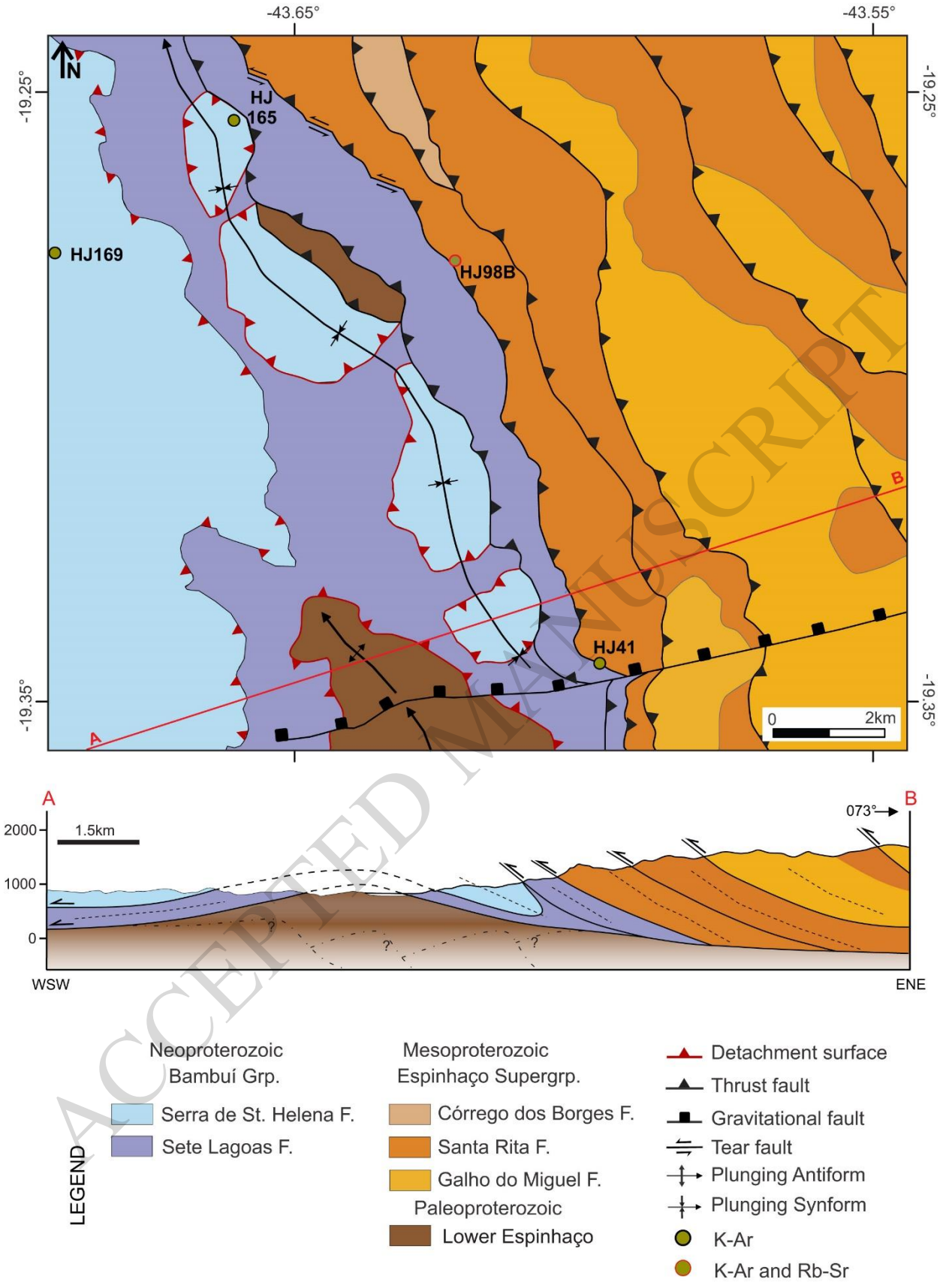

Figure 9

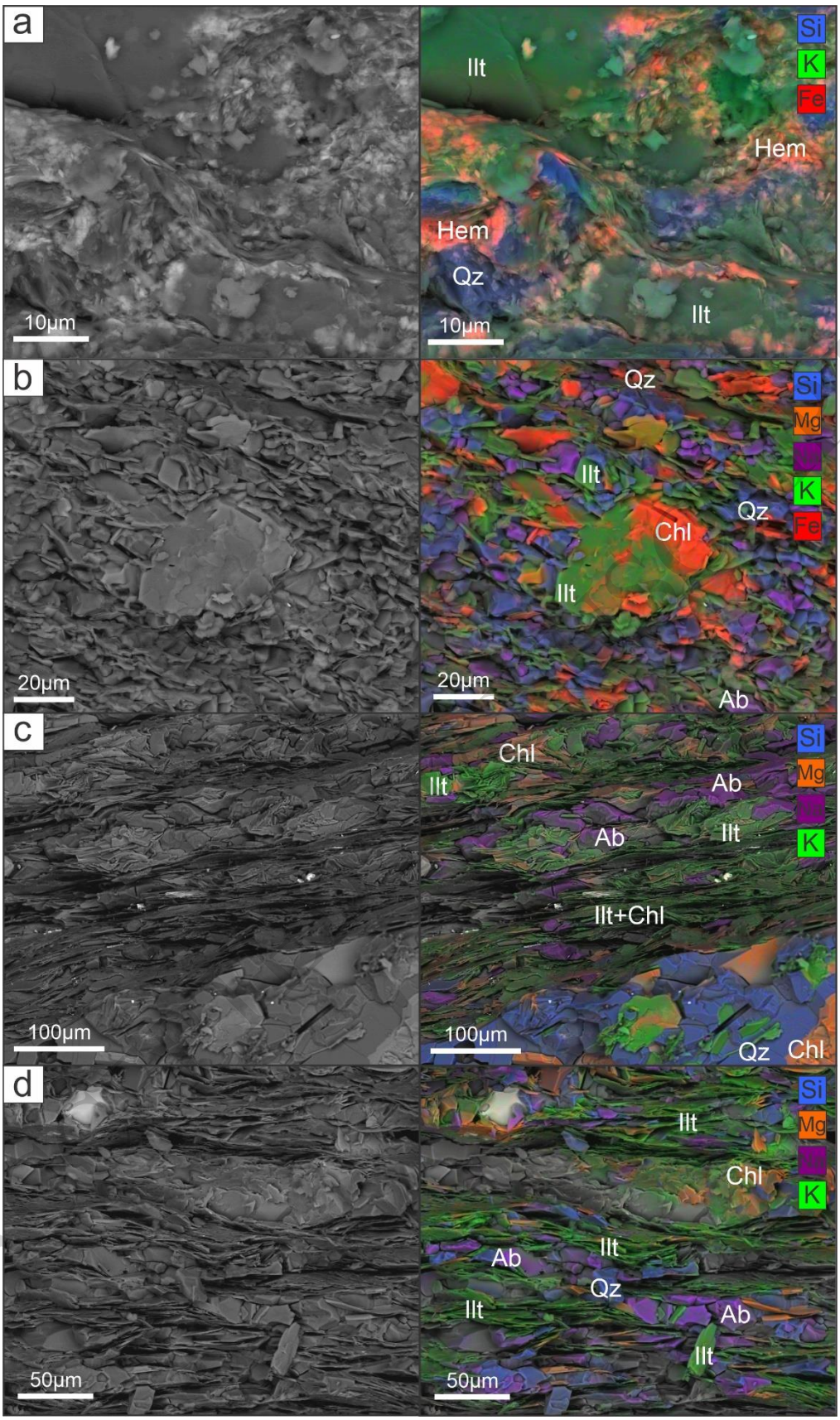

Figure 10

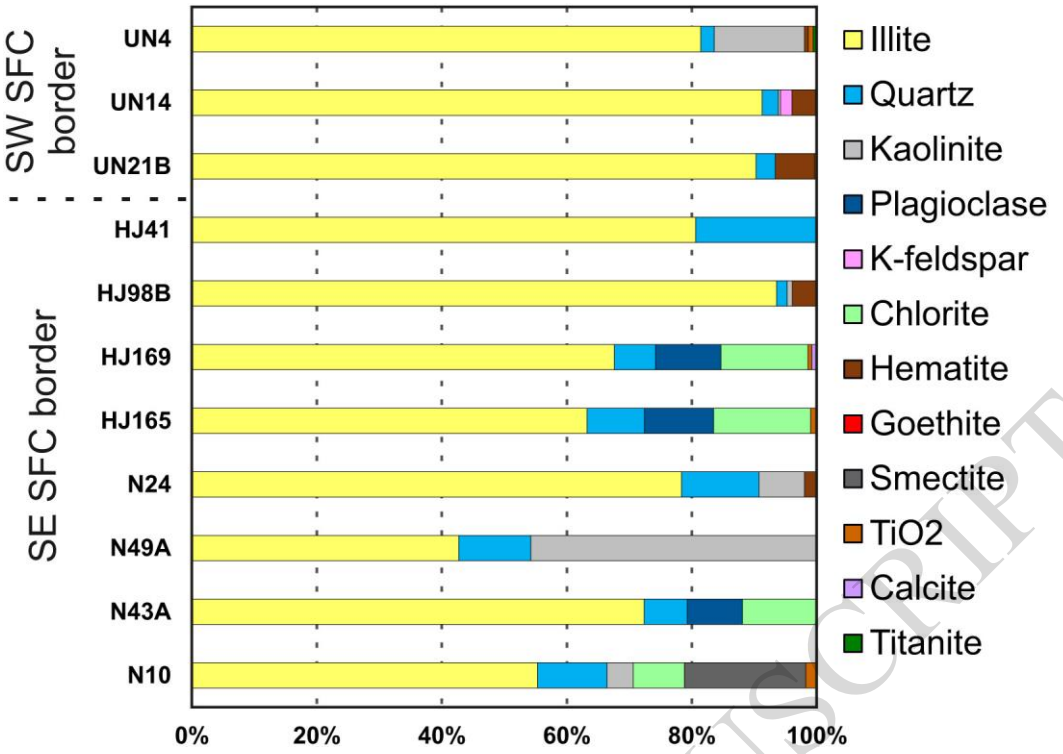

Figure 11

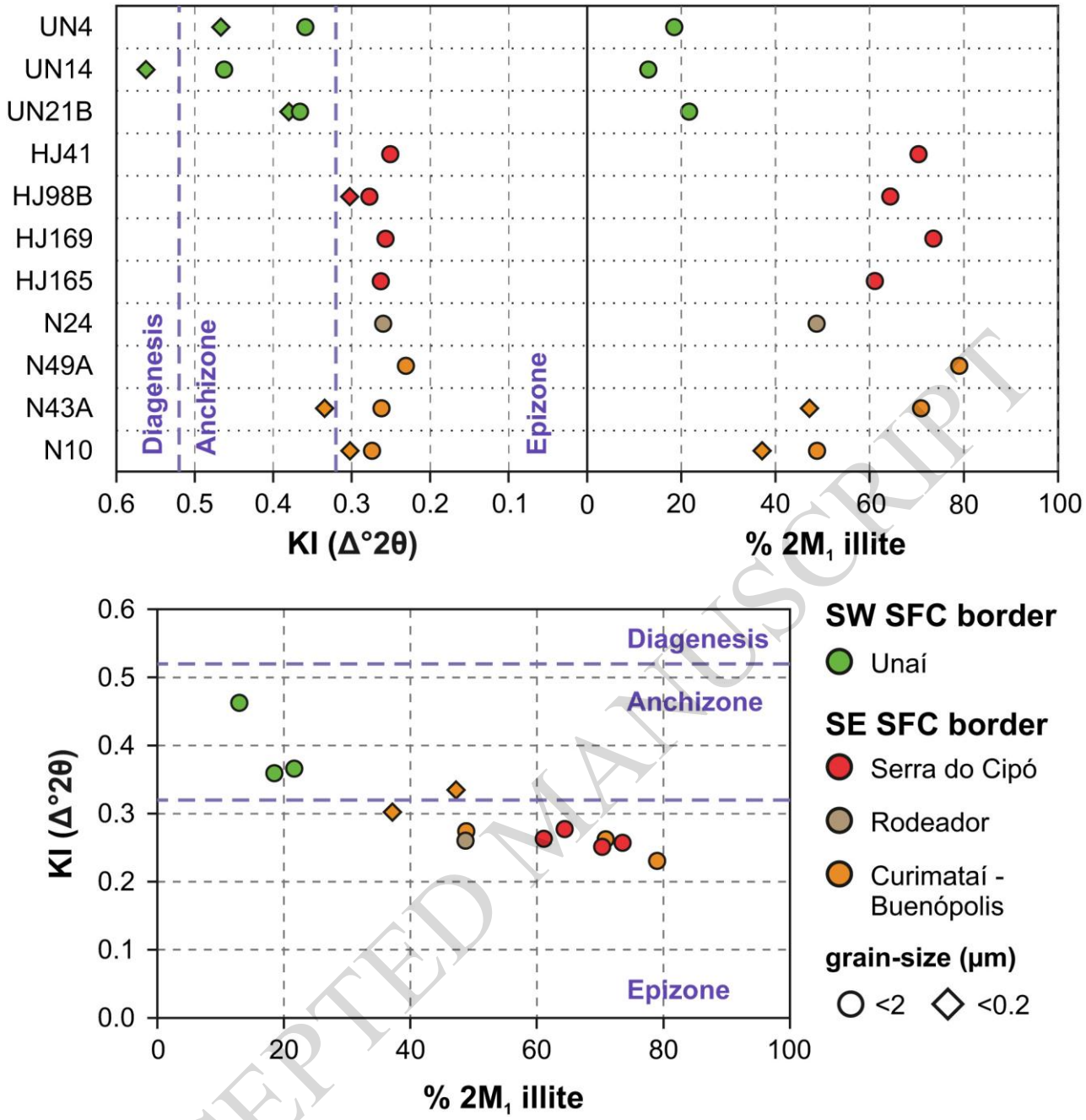

Figure 12

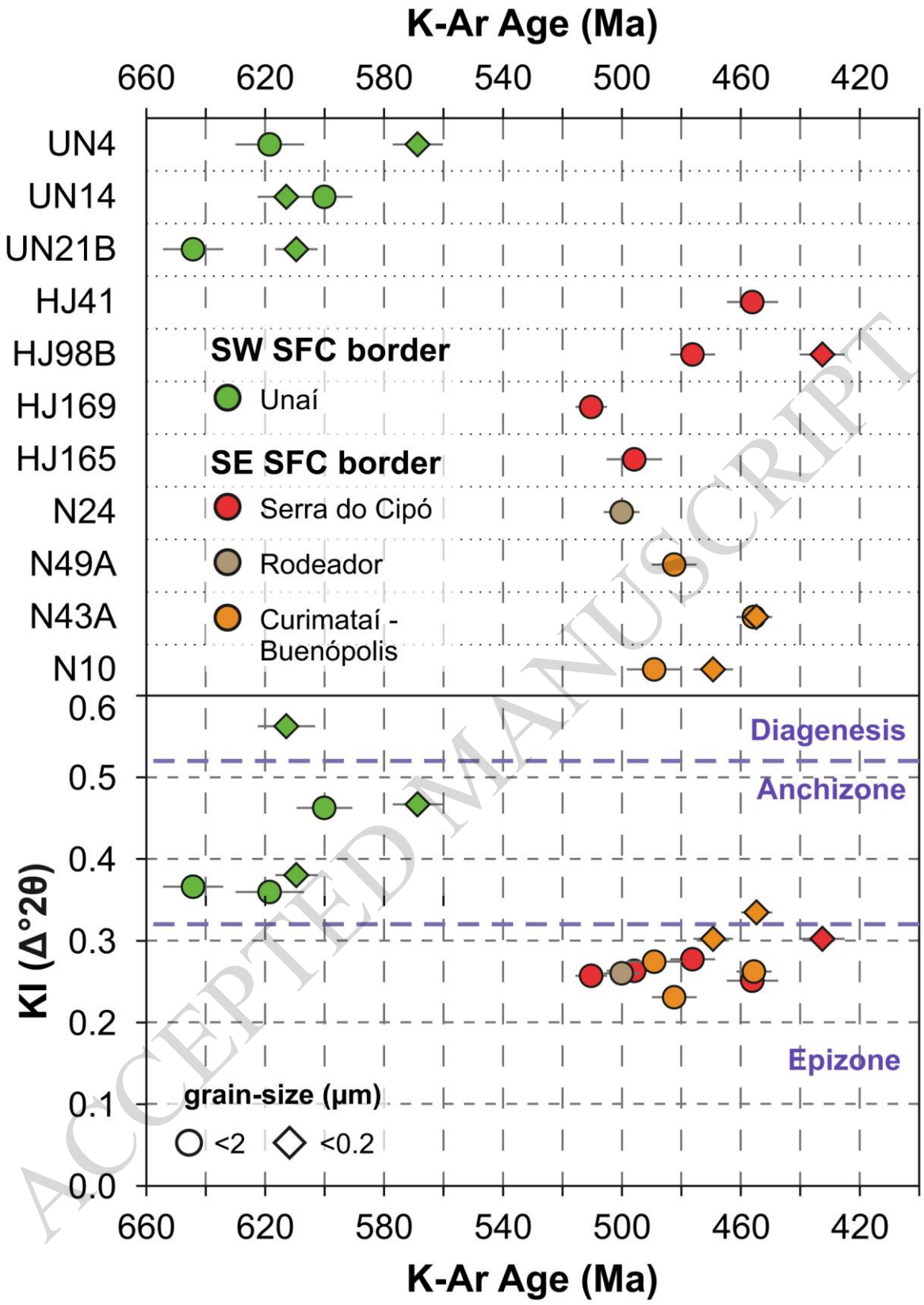

Figure 13

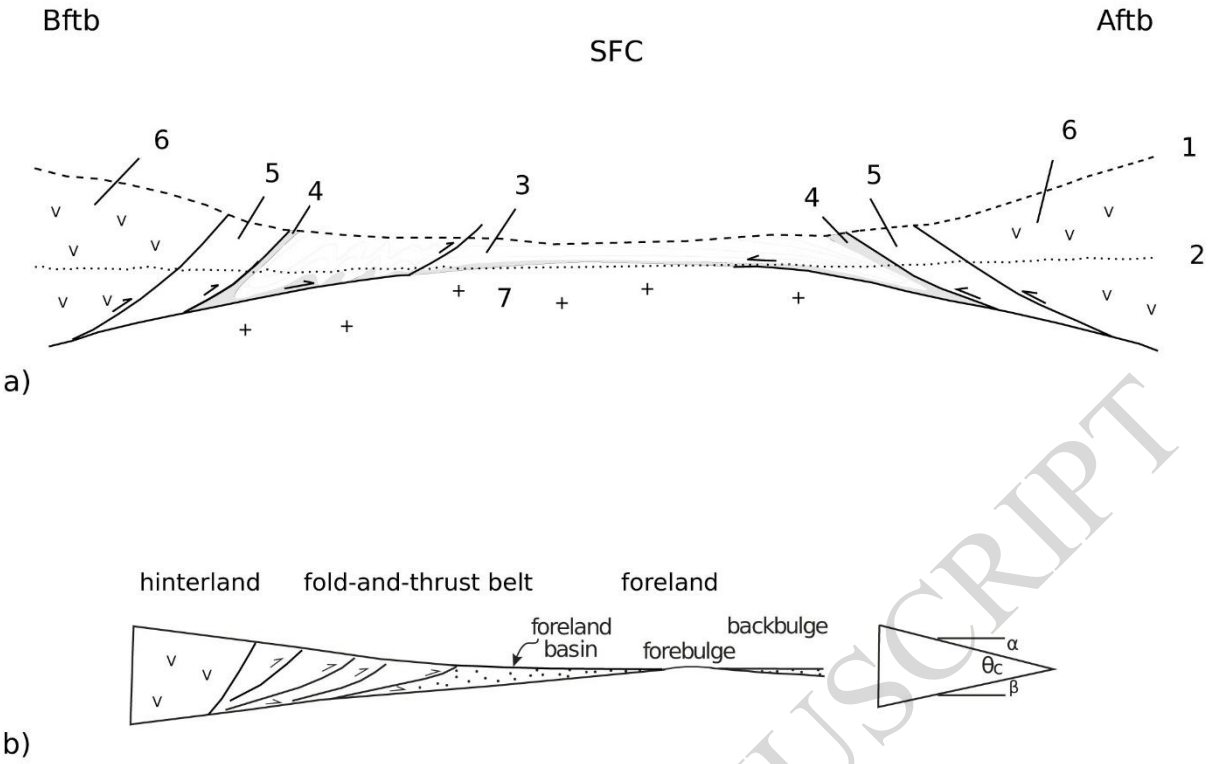

Figure 14